Nordisk kernesikkerhedsforskning
Norrænar kjarnöryggisrannsóknir
Pohjoismainen ydinturvallisuustutkimus
Nordisk kjernesikkerhetsforskning
Nordisk kärnsäkerhetsforskning
Nordic nuclear safety research

NKS-26
ISBN 87-7893-077-4

Reinforced concrete wall under hydrogen detonation

Arja Saarenheimo
VTT Manufacturing Technology
Finland

November 2000

Abstract

The structural integrity of a reinforced concrete wall in the BWR reactor building under hydrogen detonation conditions has been analysed. Of particular interest is whether the containment integrity can be jeopardised by an external hydrogen detonation. The load carrying capacity of a reinforced concrete wall was studied. The detonation pressure loads were estimated with computerised hand calculations assuming a direct initiation of detonation and applying the strong explosion theory. The results can be considered as rough and conservative estimates for the first shock pressure impact induced by a reflecting detonation wave.
Structural integrity may be endangered due to slow pressurisation or dynamic impulse loads associated with local detonations. The static pressure following the passage of a shock front may be relatively high, thus this static or slowly decreasing pressure after a detonation may damage the structure severely. The mitigating effects of the opening of a door on pressure history and structural response were also studied. The non-linear behaviour of the wall was studied under detonations corresponding a detonable hydrogen mass of 0.5 kg and 1.428 kg.
Non-linear finite element analyses of the reinforced concrete structure were carried out by the ABAQUS/Explicit program. The reinforcement and its non-linear material behaviour and the tensile cracking of concrete were modelled. Reinforcement was defined as layers of uniformly spaced reinforcing bars in shell elements. In these studies the surrounding structures of the non-linearly modelled reinforced concrete wall were modelled using idealised boundary conditions. Especially concrete cracking and yielding of the reinforcement was monitored during the numerical simulation.

Key words

Non-linear reinforced concrete, hydrogen detonation, finite element analysis

NKS-26
ISBN 87-7893-077-4

Danka Services International, DSI, 2001

The report can be obtained from

NKS Secretariat
P.O. Box 30
DK – 4000 Roskilde
Denmark

Phone +45 4677 4045
Fax +45 4677 4046
http://www.nks.org
e-mail: annette.lemmens@catscience.dk

Reinforced concrete wall under hydrogen detonation

Arja Saarenheimo

VTT Manufacturing Technology

Espoo, Finland

November, 2000

Table of contents

Acknowledgements

This report is part of the STIN (Structural Integrity) project carried out by FINNUS, the Finnish Research Programme on Nuclear Power Plant Safety. This study is funded by the Nordic Nuclear Safety Research (NKS) SOS-2 project and by the Ministry of Trade and Industry (KTM). The author is indebted to Mr. Heikki Sjövall and Mr. Timo Kukkola from Teollisuuden Voima Oy (TVO) for their technical support and review of the report. Special thanks to Ms. Ilona Lindholm and Mr. Ari Silde from VTT Energy for their co-operation during the work. Special thanks also to Mr. Kim Calonius from VTT Manufacturing Technology for performing the preliminary linear studies based on codes and standards.

Espoo, November 2000

Author

1 Introduction

This study aims to assess the structural integrity of a reinforced concrete wall during a hydrogen detonation. Hydrogen detonation leads to high, peak type pressure transients, followed by a relatively high, slowly decreasing pressure. Structural integrity can be endangered due to slow pressurisation or dynamic impulse loads associated with local detonations.

Shock pressure transient loads typical of hydrogen detonation are evaluated with the DETO code. This code is based on the strong explosion theory, taking into account the pressure effects of both the incident shock wave and the first shock reflection from the structure. Propagation of the combustion front of detonation is not treated. Instead, the code models the propagation of an adiabatic shock wave induced by point-like energy release, and the first reflection of the shock from the wall structure. A program interface between DETO 2.0 and ABAQUS/Explicit codes has also been developed at VTT Energy. This program provides a flexible data transfer between these codes.

Preliminary linear structural analyses were carried out by the ABAQUS/Standard program. Eigenmodes and natural frequencies of the model were evaluated. Also, the capacity of the reinforced concrete wall under constant pressure was predicted by linear and non-linear methods. Materially non-linear static analyses were carried out using the reinforced concrete model available in the ABAQUS/Standard Finite element method program.

Non-linear dynamic finite element analyses of the reinforced concrete wall were carried out by the ABAQUS/Explicit program. The reinforcement and its rate-dependent elastic-plastic material behaviour, as well as the tensile cracking of concrete, were modelled.

2 Preliminary studies

2.1 Finite element model

The geometric model showing the main dimensions and FE mesh is represented in Figures 2.1, 2.2 and 2.3 for the three topmost floors of the reinforced wall in the shaft and part of the connecting structure. Since the wall and its supporting framework are horizontally nearly symmetrical, only half the structure is modelled. The X-Y (1-2) plane is the symmetry plane. All modelled floors and walls are assumed to be rigidly joined. Figure 2.1 also shows the locations of the detonation points. Also, the location of the model used in non-linear analyses is indicated.

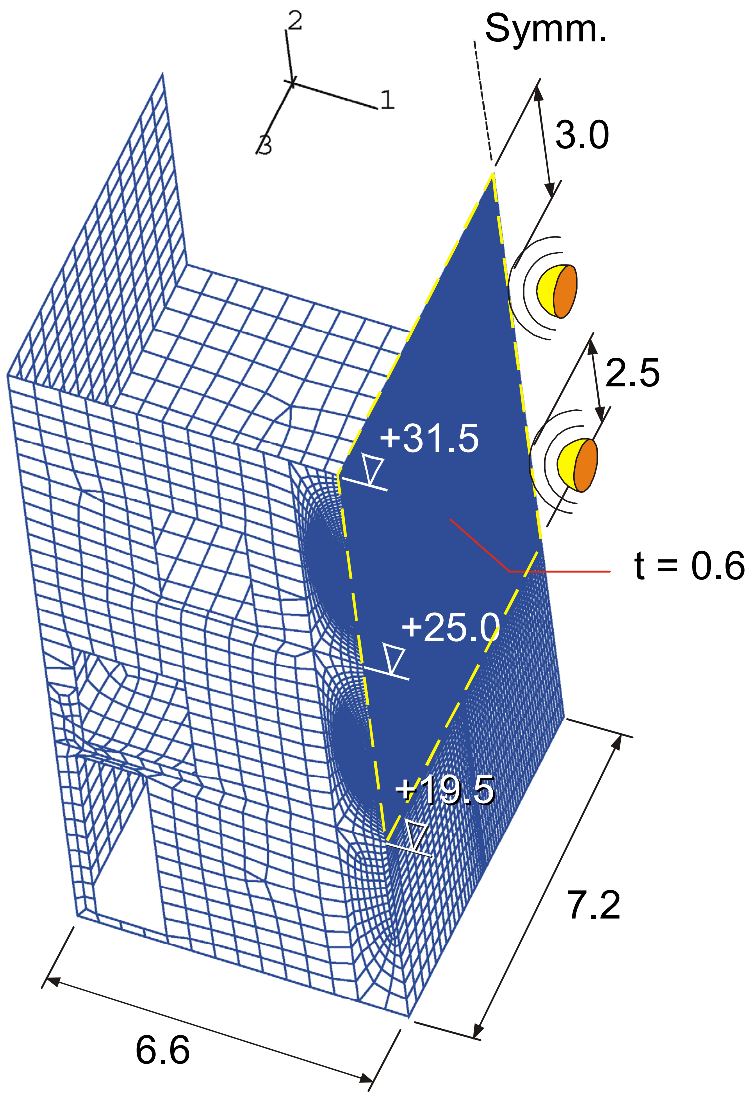

Figure 2.1. Finite element model of the structure. Locations closest to the upper and lower detonation point indicated by circles. The dashed line indicates the location of the non-linear FE-model.

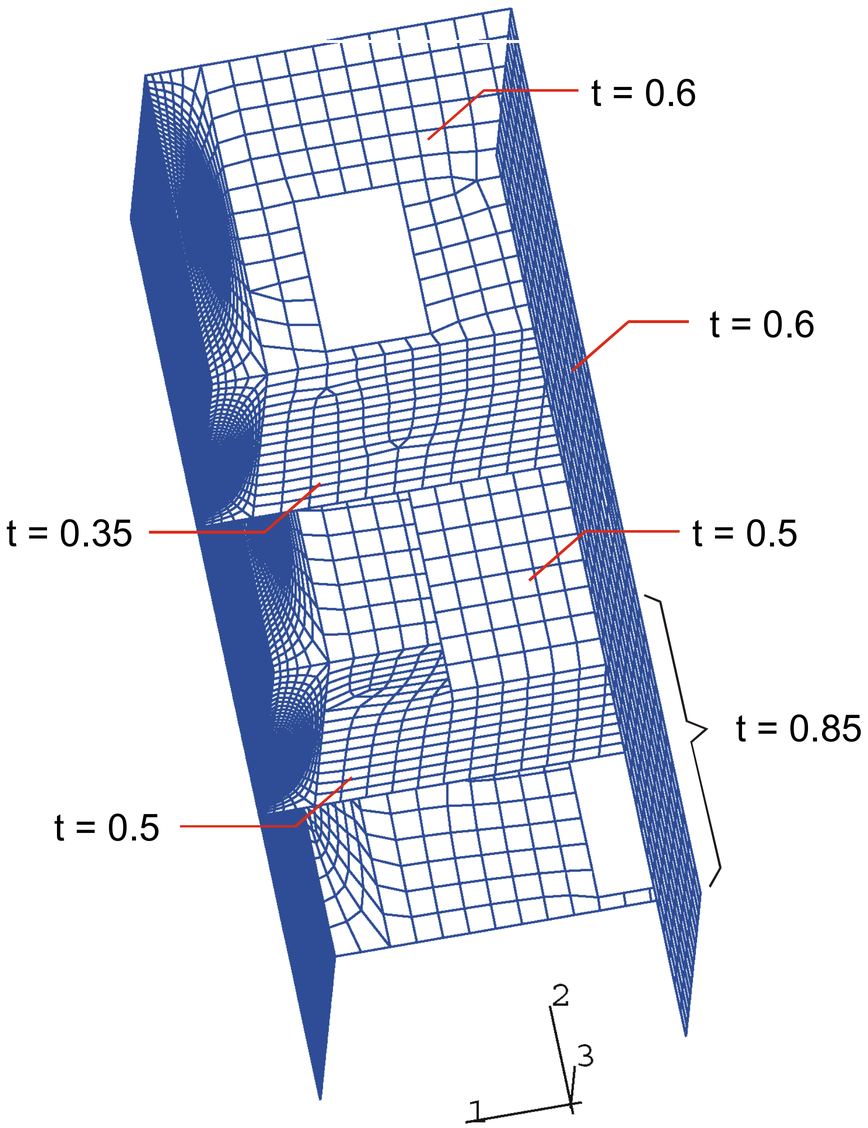

Figure 2.2. FE Model. t is the thickness of the structure.

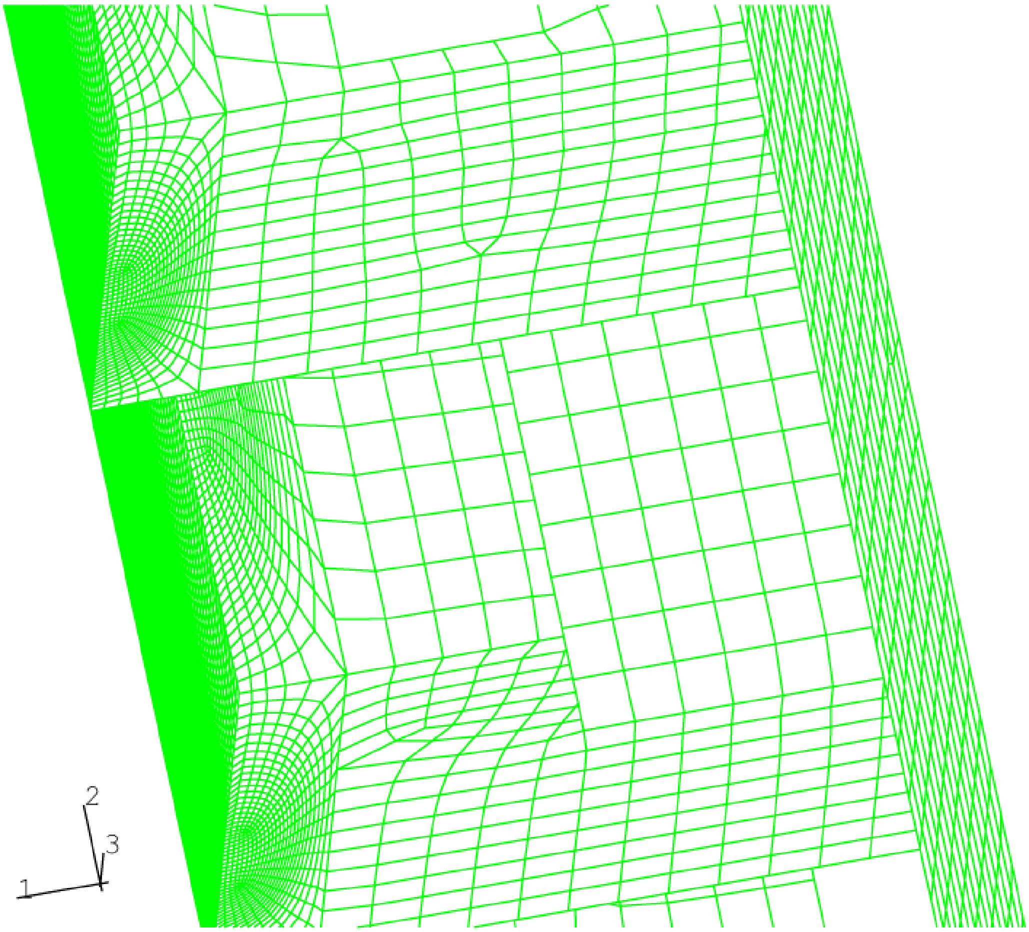

Figure 2.3. Detail of the FE model.

In preliminary studies, the whole structure is assumed to be a homogeneous material. For static analyses and the natural frequency extractions the following three material parameters are needed:

Density

$$\rho_c = 2500 \frac{kg}{m^3}$$

Young's Modulus

$$E_c = 5000k\sqrt{K}\,, \tag{2.1}$$

where $k = \dfrac{\rho_c}{2400}$, but also $k \le 1.0$. The nominal strength $K = 30\dfrac{MN}{m^2} = 30 \cdot 10^6 \dfrac{N}{m^3}$.

Now, $k = 1.0$ and

$$E_c = 5000 \cdot \sqrt{30}\frac{MN}{m^3} = 27386\frac{MN}{m^3} = 2.7 \cdot 10^{10}\,Pa \quad .$$

Since the concrete is reinforced throughout the system, an equivalent E_c^{eq} has to be defined. It is a weighted mean value of the moduli of concrete and steel. On average the concrete reinforcement is ∅ 16 k 250 near the upper and the lower surfaces, in the direction of the load. The average thickness of the wall is 0.6 m. Thus in 1 cubic meter the volume of the steel is

$$V_s = 2\cdot\pi\left(\frac{0.016}{2}\right)^2\cdot\frac{1000}{250}/0.6 = 2.681\cdot 10^{-3}\,m^3 \tag{2.2}$$

and the equivalent Young's Modulus for the reinforced concrete is

$$\begin{aligned} E_c^{eq} &= (1-0.002681)\cdot 27386MPa + 0.002681\cdot 200000 \\ &= 27313MPa + 536MPa = 27849MPa \approx 2.8\cdot 10^{10}\,Pa \end{aligned} \tag{2.3}$$

2.1.1 Loads and boundary conditions

In the following there are three main variations in respect of boundary conditions, termed Case 1L, Case 2L and Case 3L. Letter L refers to the analysis type, which is linear. In all these cases the X-Y plane is the symmetrical plane. Thus every node in that plane has three degrees of freedom: translation in the Z direction and rotations around X and Y axes. With those conditions alone, however, the system would be statically indeterminate. Thus additional constrictions are introduced: In Case 1L the lowest floor level is completely rigid, and all six degrees of freedom are fixed in these nodes. In Case 2L also the downmost level of the left wall edge is rigid. In Case 3L the two first levels of that particular edge are rigid as shown in Figure 2.4, meaning approx. 2/3 of the whole height of the examined structure.

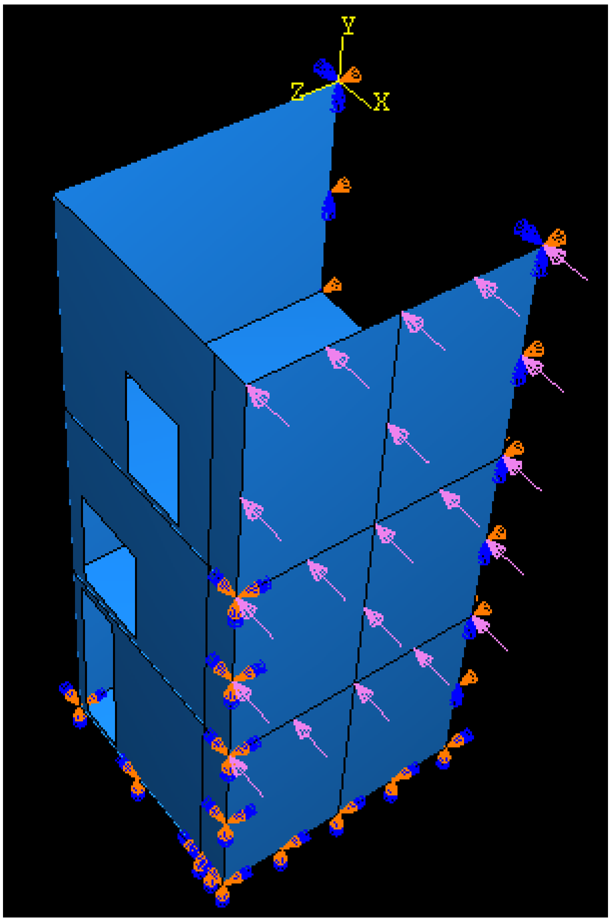

Figure 2.4. Load and boundary conditions of the model. Case 3L.

In all these cases the loading is a constant pressure on the wall considered. It is defined in Chapter 2.4. Figure 2.4 shows the load and boundary conditions. Constant pressure load is indicated with pink arrows.

Also, a finite element model of the wall was used in non-linear analyses. Only the loaded part of the geometry shown in Fig. 2.1 was modelled. A simplified model was formulated by removing surrounding elements and composing these parts of the model with boundary conditions. The supporting vertical wall and supporting vertical structures at level 19.0 m were modelled as fully fixed. The floor at level 25.0 m was modelled assuming the displacement of the wall at level 25.0 m along the global 1-axis to be zero. These models are referred to in the following as Wall.

2.2 Eigenmodes

The first 20 natural frequencies and corresponding mode shapes of the system are calculated in Case 1. The lowest natural modes, their frequencies and generalised masses are given in Table 2.1. The first five mode shapes are shown in Figures 2.5 - 2.7.

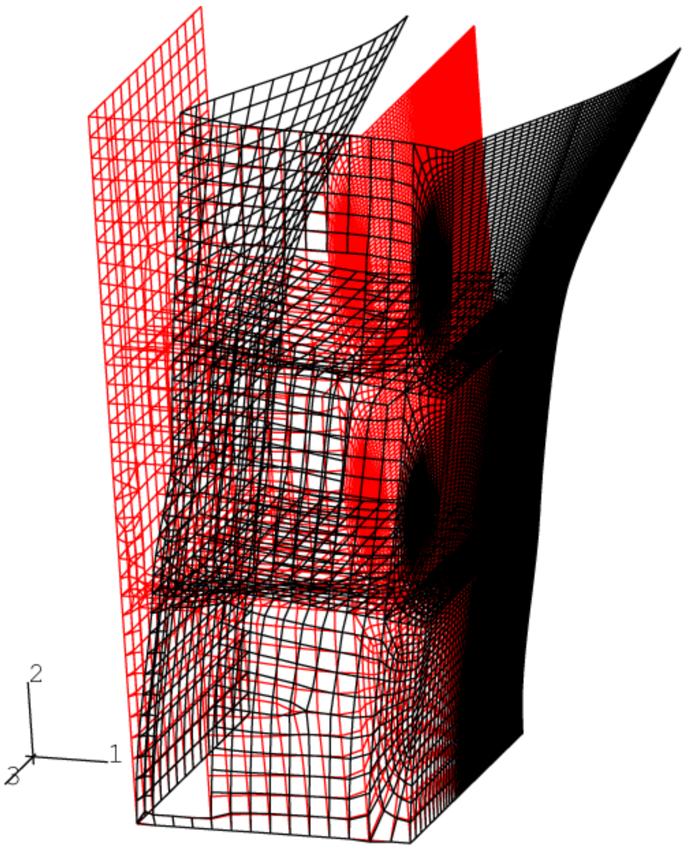

Figure 2.5. Mode shape 1 (amplitude of oscillation). The corresponding frequency is 8.2933 Hz. Undeformed shape in red.

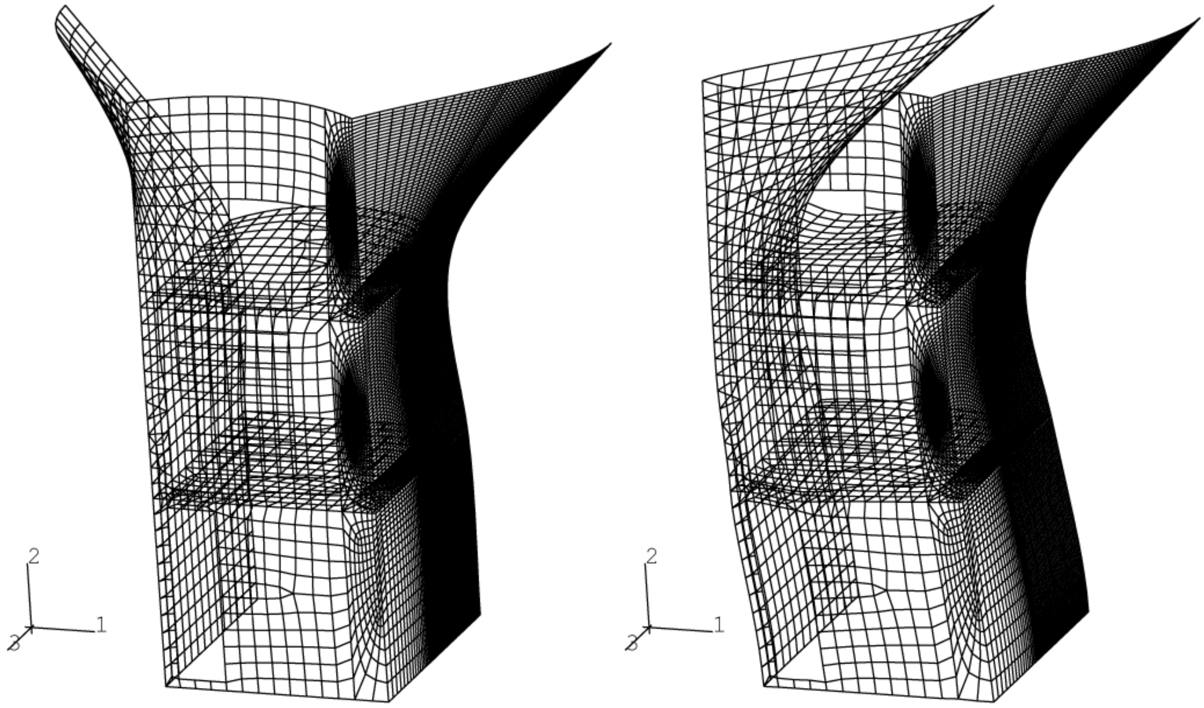

Figure 2.6. Mode shapes 2 and 3 (amplitudes of oscillation). The corresponding frequencies are 12.412 Hz and 15.460 Hz.

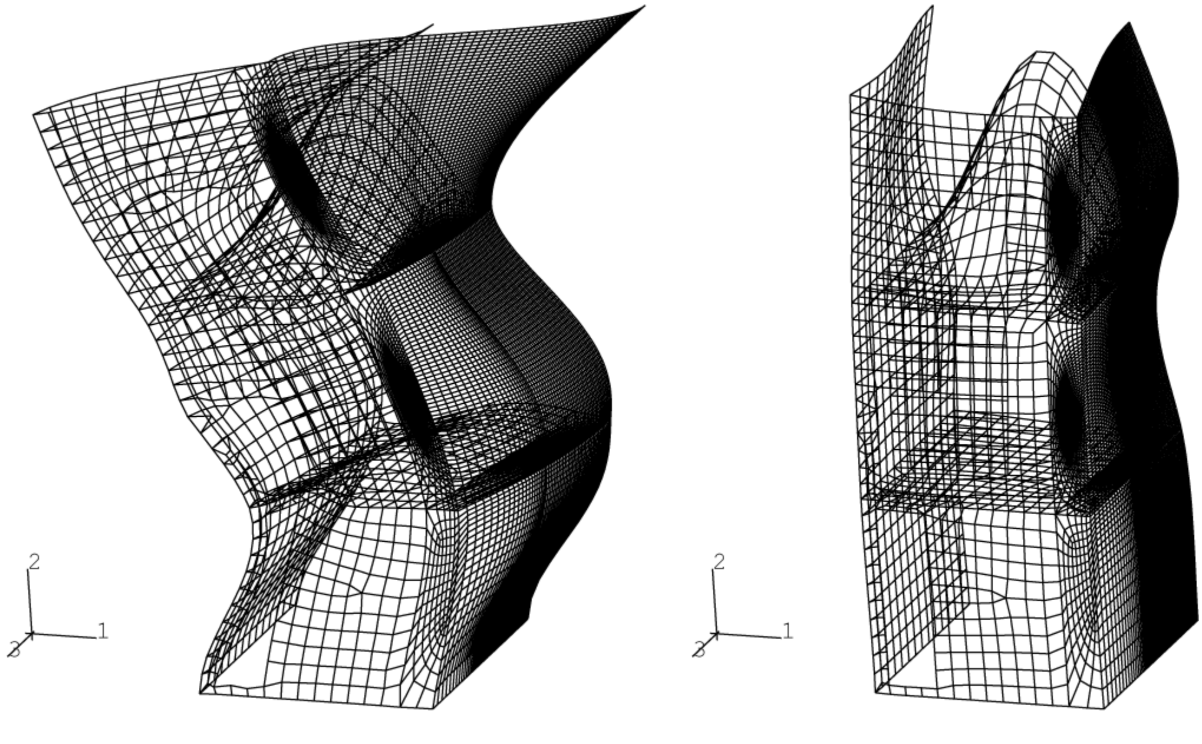

Figure 2.7. Mode shapes 4 and 5 (amplitudes of oscillation). The corresponding frequencies are 28.902 Hz and 30.515.

The lowest eigenfrequencies of the model used for linear considerations and corresponding values of the model of the wall are given in Table 2.1.

Table 2.1. Eigenfrequencies [Hz].

Mode	Linear Model	Wall only
1	8.2933	14.5
2	12.412	46.9
3	15.46	56.3
4	28.902	62.4
5	30.515	85.5

For conservative reasons and due to computational capacity limitations the Wall-only model was used in non-linear analyses.

2.3 Moment capacities

The moment capacities of three critical areas in the studied reinforced wall were defined. The critical areas are evaluated in the next chapter by examining the moment distributions in the case of a unit pressure load. The ultimate strength design is based on Finnish concrete norms B4 (1987). The structural class is 1. First, the design strengths of the steel and concrete are defined. Service strength is divided by the partial safety coefficient.

Steel A400H

Ultimate yield strength

$$f_{yd} = \frac{f_{yk}}{\gamma_s} = \frac{400}{1.1} = 364MPa \tag{2.4}$$

Concrete K30

The following two values were obtained from the Finnish Concrete Standard (Betoninormit 1981).

Ultimate compressive strength

$$f_{cd} = 15.6MPa$$

Ultimate tensile strength

$$f_{ctd} = 1.43MPa$$

Initially, the wall cross-section and the reinforcement is known. The protective screed of both the main reinforcement and the compression reinforcement is 20 - 45 mm and is simplified to a constant value of 30 mm. Since the reinforcement bars are 16 mm in diameter, the distance of the inner tensile force from the compression side is

$$d = 0.6 - 0.03 - \frac{0.016}{2} = 0.562m \tag{2.5}$$

The corresponding distance of the compressive force is

$$d' = 0.03 + \frac{0.016}{2} = 0.038m$$

Since the ratio of compression and tension in the surfaces is approximately 8 to 10 in every critical area (according to the stress results in Chapter 2.4), the height of the compression side is calculated as follows:

$$\frac{x}{h-x} = \frac{8}{10} \Rightarrow x = \frac{4}{9}h = 0.267 \tag{2.6}$$

First, the bending strength M_u has to be defined. Only after that is the compression reinforcement relevant. A section length of 1 m is considered.

$$\begin{aligned} M_u &= A_s f_{yd} z = A_s f_{yd} d\left(1 - \frac{\beta}{2}\right) = A_s f_{yd} d\left(1 - \frac{y}{2d}\right) = A_s f_{yd} d\left(1 - 0.4\frac{x}{d}\right) \\ &= 166 \cdot A_s \end{aligned} \tag{2.7}$$

The main reinforcement area has to be given in square meters for a 1 m breadth of wall section. Table 2.2 shows the main reinforcement related to the direction of the critical moment and the corresponding steel area and bending capacity of the critical regions. The first critical region is the upper left corner of the wall. The second critical region is the upper right corner, which is at the symmetry line of the model. Both regions are critical in the horizontal bending. The third region is critical in vertical bending and lies at the junction of the wall, the floor (level 25.00) and the symmetrical plane.

Table 2.2 Ultimate bending capacity in critical regions.

crit. region	main reinf. [mm]	steel area [m^2]	M_u [MNm/m]
1	16k125	0.001608	0.267
2	16k250	0.000804	0.134
3	16k325	0.000619	0.103

If the moment is higher than the ultimate bending moment, the main reinforcement starts to yield and the concrete cracks on the tensile side. Next, the structure has to be checked against compression. The ultimate bending strength of a structure with compression reinforcement is the sum of the compressive strength of both the concrete and compressive reinforcement: The compression capacity of this, rather weakly reinforced, wall becomes non-critical.

2.4 Unit pressure

A static FEM analysis is run to determine the displacements, stress and moment distribution. The loading is a pressure of 1 bar (0.1 MPa) in the negative direction of the X axis. The loaded area is the two uppermost levels of the wall and is shown in Figure 2.5. Figure 2.8 shows the displaced shape of the wall under a constant pressure load, Case 2L. The von Mises stress distribution throughout the model is shown in Fig. 2.9.

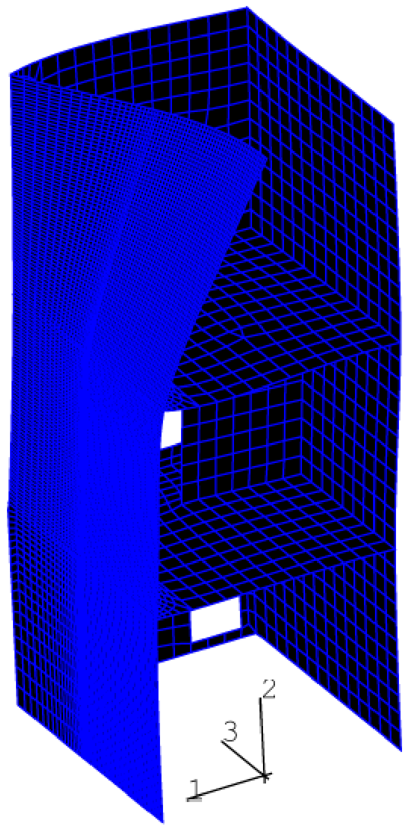

Figure 2.8. Displaced shape of the model. Case 2L.

The horizontal stress distribution at the outer surface of the wall in Case 1L is shown in Fig. 2.10. The surface at which the pressure is acting is referred to as the inner surface. Vertical stresses at the inner surface of the wall are shown in Fig. 2.11. As can be seen, the ultimate tensile stress of the concrete is exceeded near the supporting areas at the inner surface and at the outer surface near the symmetry line.

The horizontal bending moment distribution in Case 1L is shown in Fig. 2.12 and the vertical bending moment distribution in Fig. 2.13. The horizontal displacement distribution in the 1-axis direction is presented in Fig. 2.14.

The horizontal bending moment distribution in Case 3L is shown in Fig. 2.15 and the vertical bending moment distribution in Fig. 2.16. The horizontal displacement distribution in the 1-axis direction is presented in Fig. 2.17.

The moments in the critical regions and critical direction are listed in Table 2.3. There are no significant differences in the bending moment distributions in the studied Cases 1L-3L.

Since the moment is directly proportional to the pressure load, the design moment can be derived by superposition:

$$M_d = \gamma \cdot M = 1.0 \cdot M \qquad (2.8)$$

where $\gamma = 1$ in accident load cases.

Table 2.3. Bending moment at critical regions.

crit. region	M_d [MNm/m]
1	0.5
2	-0.4
3	0.5

The load capacity of the wall can be defined by comparing the moments in the case of unit load and the corresponding bending capacity (Table 2.2). The most critical region is thus Region 3 and the maximum load capacity for uniformly distributed load in the wall is

$$p_d = \frac{M_u}{M_d} \cdot 1 = \frac{0.103}{0.5} = 0.206 bar \qquad (2.9)$$

Thus, when the load exceeds 0.206 bar, the main reinforcement starts to yield.

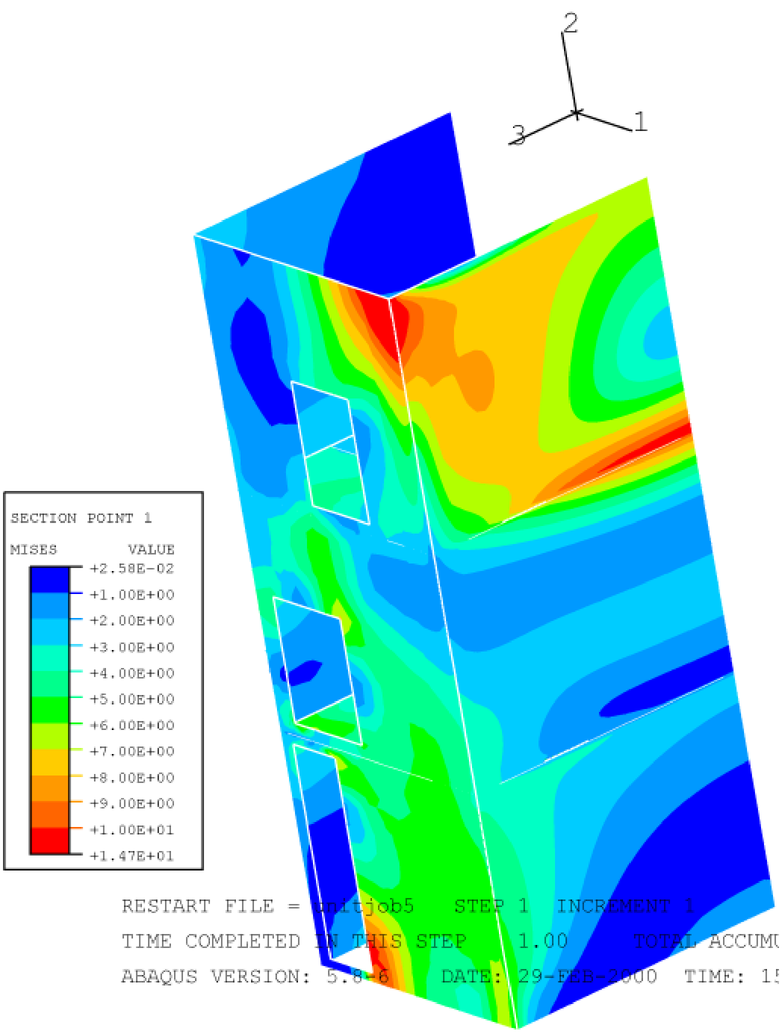

Figure 2.9. Contour plot of the von Mises stress distribution (max. 14.7 MPa throughout the model, section point 1 (inner surface), Case 1L.

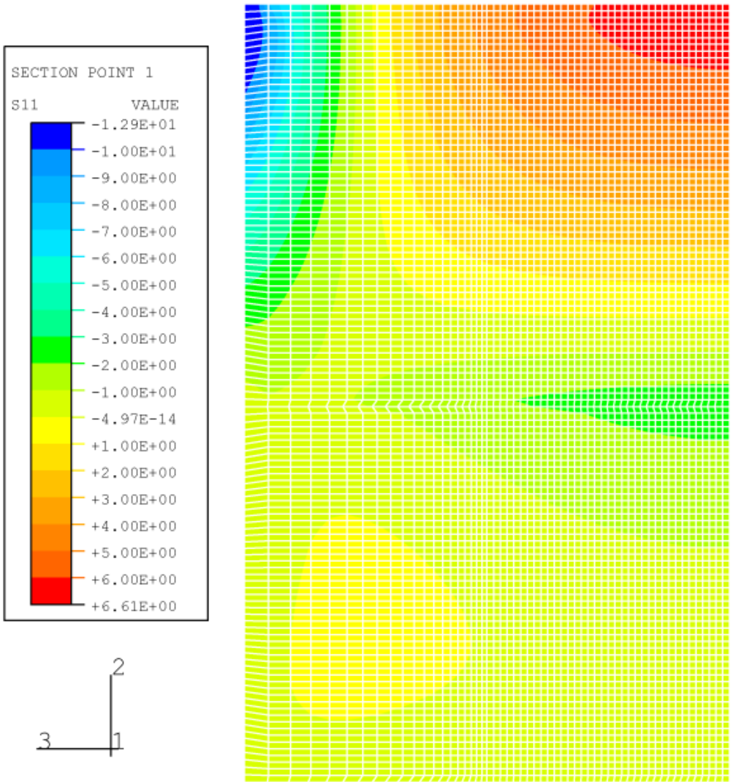

Figure 2.10. Contour plot of the horizontal stress (σ_{11}) distribution (min.-12.9 MPa, max. 6.6 MPa) in the wall, section point 1, Case 1L.

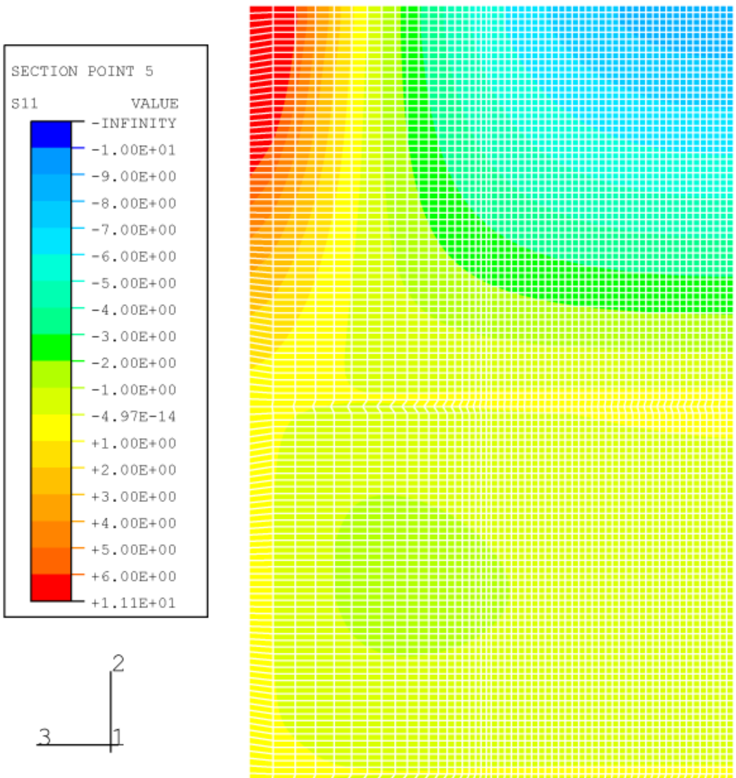

Figure 2.11. Contour plot of the vertical stress (σ_{11}) distribution (min. -10 MPa, max. 11.1 MPa) in the wall, section point 5, Case 1L.

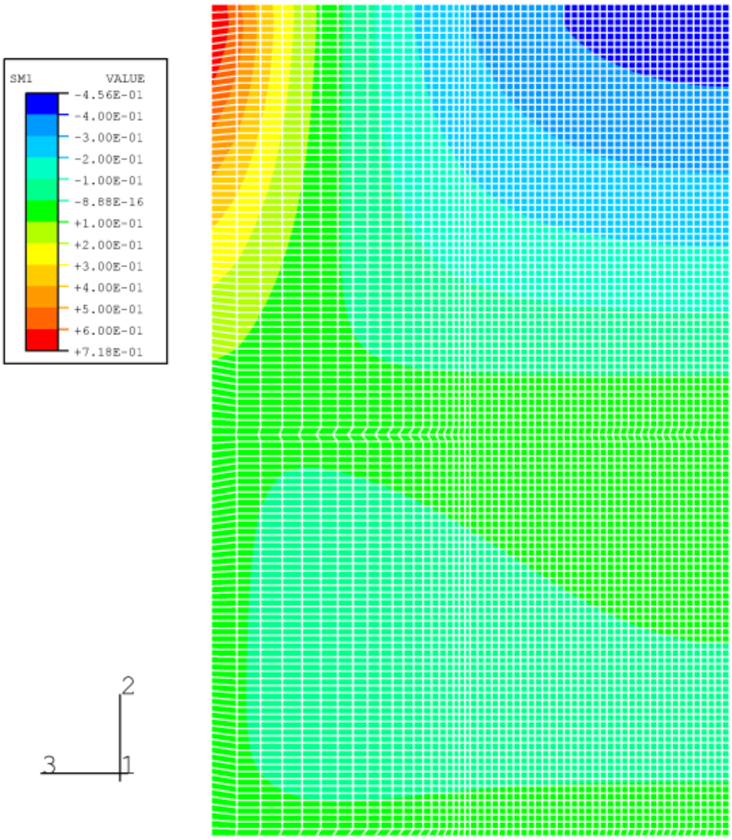

Figure 2.12. Contour plot of the horizontal moment (M_1) distribution (min. -0.45 MNm/m, max. 0.71 MNm/m) in the wall, Case 1L.

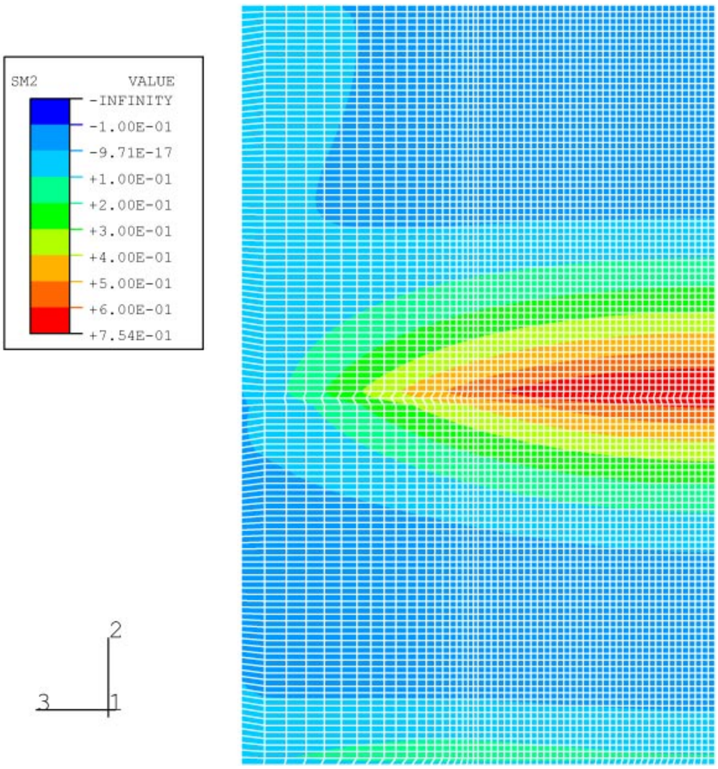

Figure 2.13. Contour plot of the vertical moment (M2) distribution (min. -0.1 MNm/m, max. 0.75 MNm/m) in the wall, Case 1L.

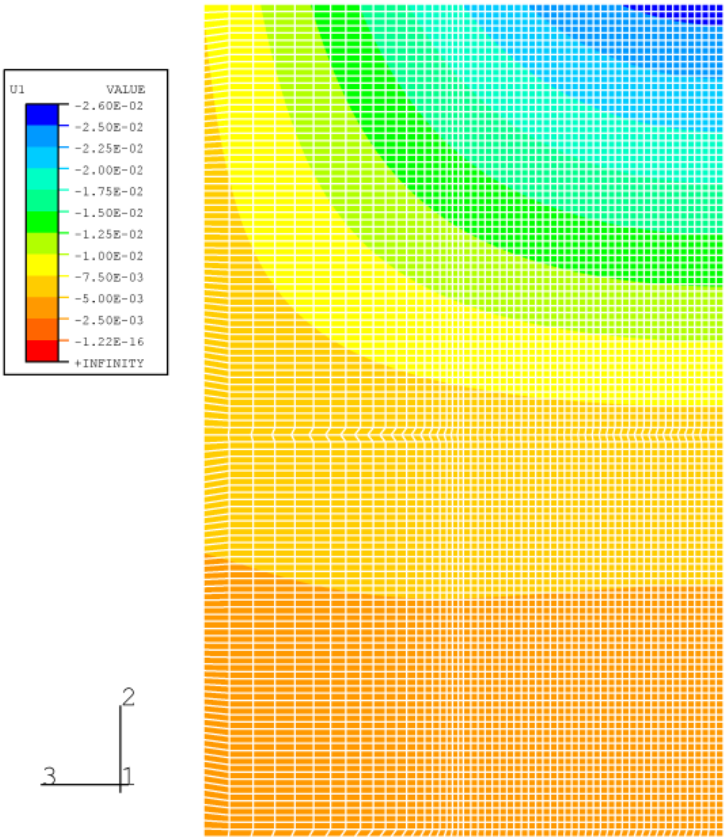

Figure 2.14. Contour plot of the displacements (m) in the normal direction (u_1).

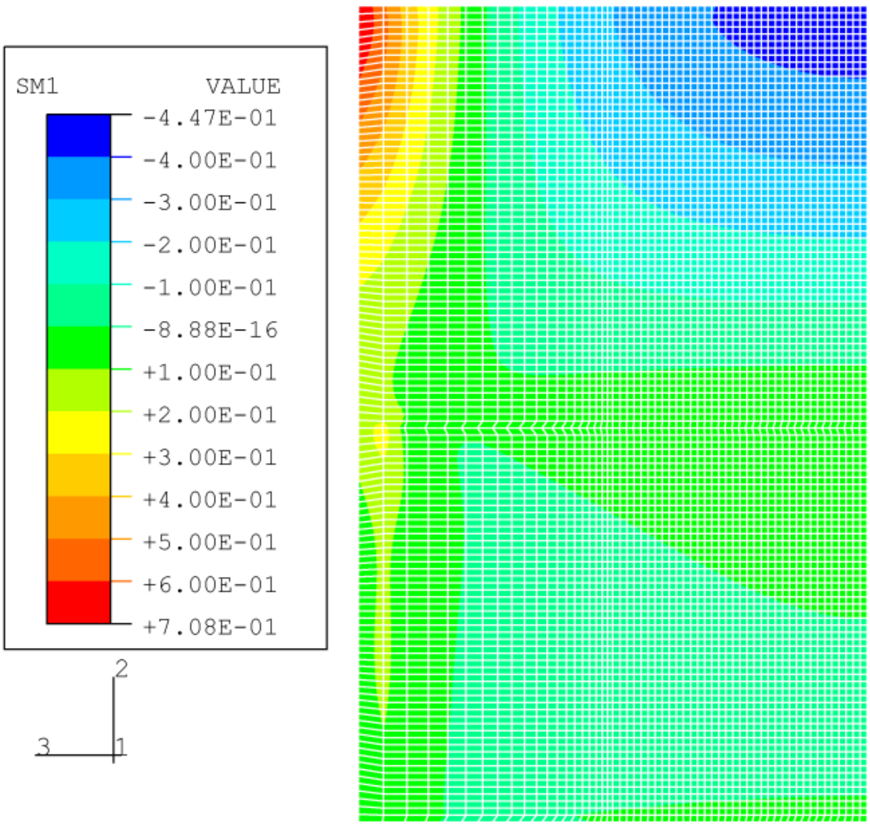

Figure 2.15. Contour plot of the horizontal moment distribution (min. -0.45 MNm/m, max. 0.7 MNm/m) in the wall, Case 3L.

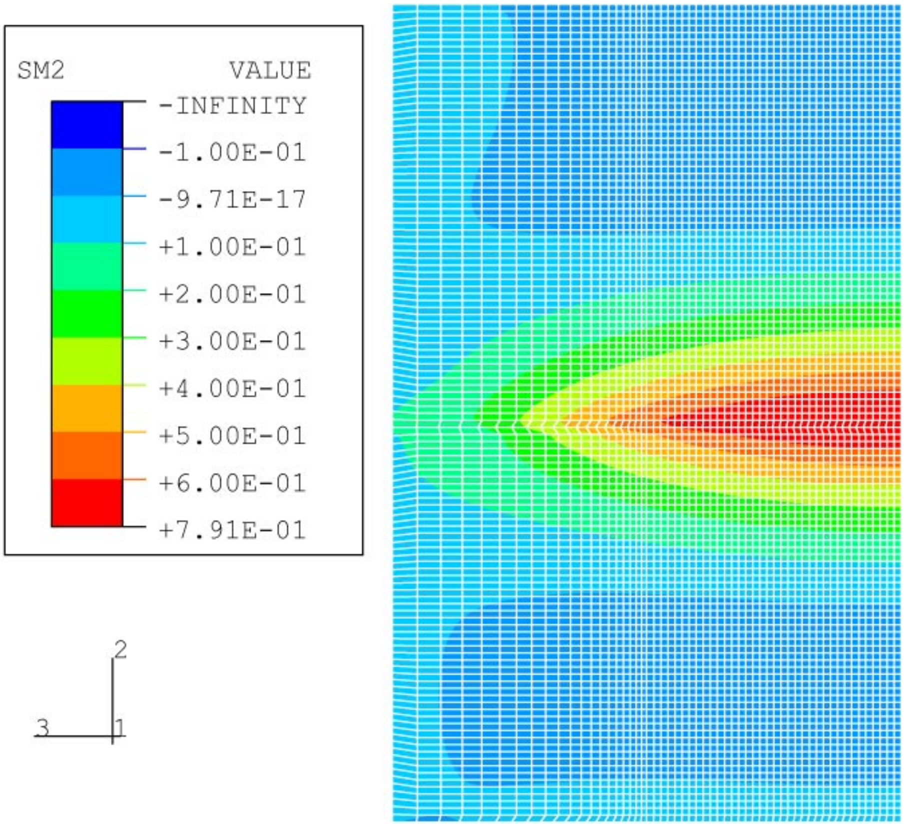

Figure 2.16. Contour plot of the vertical moment distribution (min. -0.1 MNm/m, max. 0.8 MNm/m) in the wall, Case 3L.

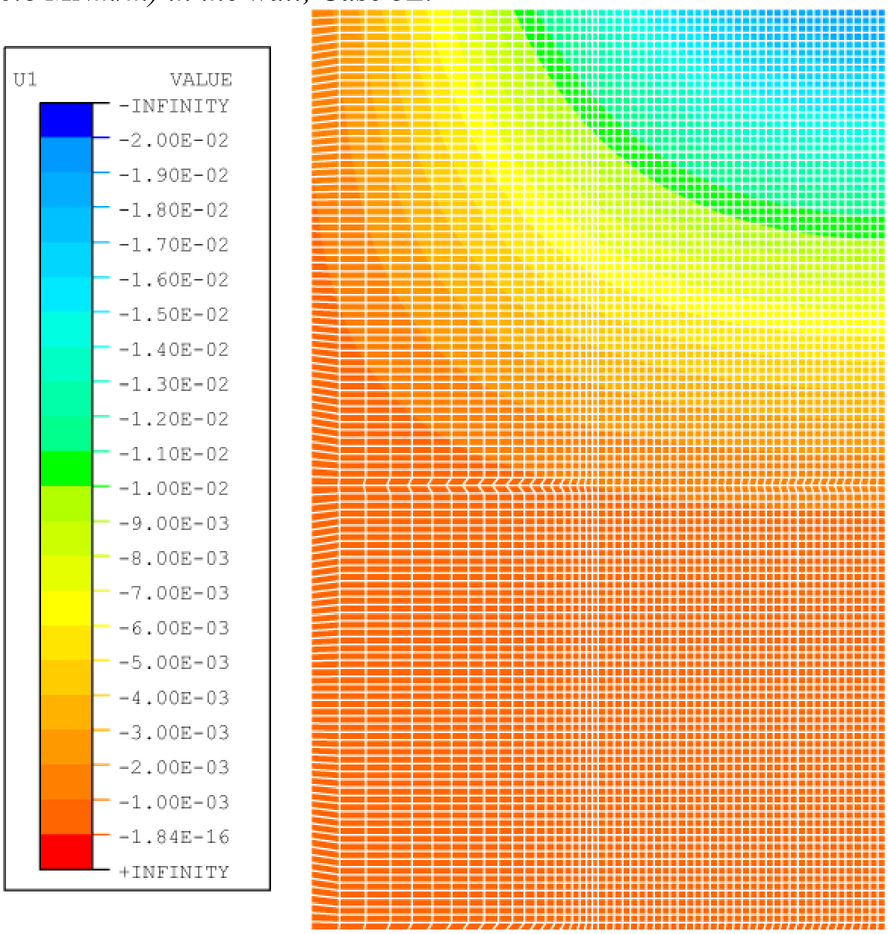

Figure 2.17. Contour plot of the displacements (m) in the normal direction, Case 3L.

Wall model

Linear moment distributions of the wall model under constant pressure are not shown here. Compared to the previously presented results, the horizontal moment distribution (around the 2-axis) overestimates the moment on the support. This is, of course, due to the fully fixed rotational degrees of freedom along the edge. At any rate, the fully fixed assumption is more conservative. On the other hand, the results of Cases 1L, 2L and 3L may underestimate the support moment. Moment distributions related to the vertical direction (around the 3-axis) are similar in Cases 1L-3L and in the wall model. For a number of reasons only the wall model is used in further non-linear analyses.

3 Non-linear analyses

The FE mesh used in the following analyses is shown in Figs 2.10 - 2.17. There are about 6500 four-noded shell elements. This element, referred to as S4R in ABAQUS Manuals, is a double curved shell element with hourglass control and reduced integration. In these analyses five calculation points were used through the element thickness.

3.1 Material modelling of reinforced concrete

Concrete

Concrete withstands primarily compression and its tensile strength is typically one tenth of the compression strength. The response of concrete to uniaxial and combined stresses is non-linear due to progressive microcracking at the transition zone between the aggregates and the bulk cement paste. Yielding and failure surfaces in the biaxial stress state are shown in Fig. 3.1. Uniaxial behaviour of concrete is shown in Fig. 3.2.

The ABAQUS/Standard program provides a more general capability for modelling concrete due to the elastic-plastic yield theory applied for dominantly compressive stress components. Also, this model simplifies the actual behaviour especially when the concrete is strained beyond the ultimate stress point. Open tensile cracks are modelled by a loss of elastic stiffness. The cracks may close if the stress across them becomes compressive.

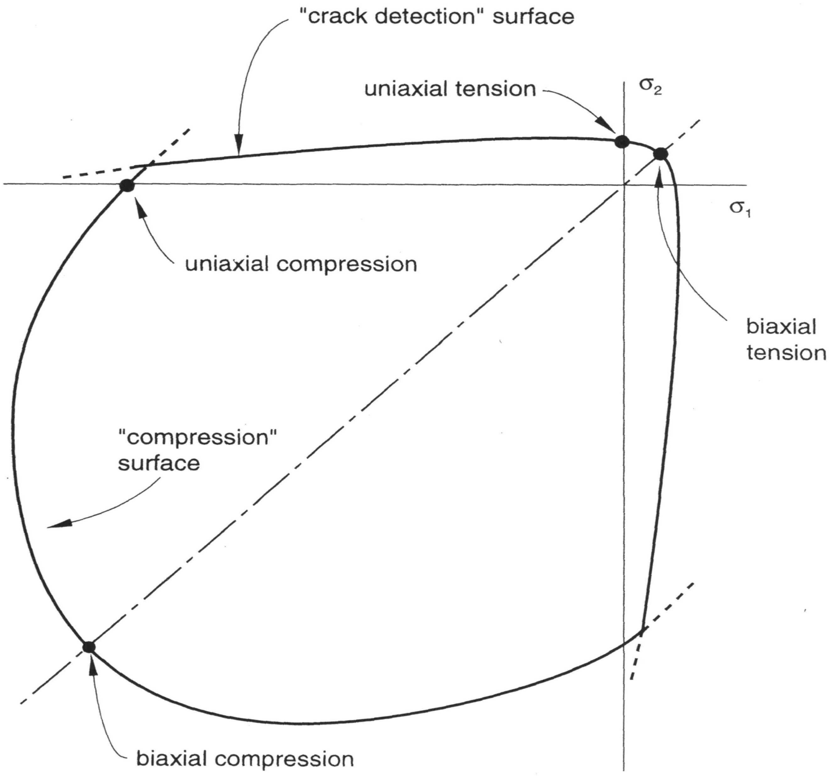

Figure 3.1. Yield and failure surfaces in plane stress (ABAQUS Theory Manual 1998).

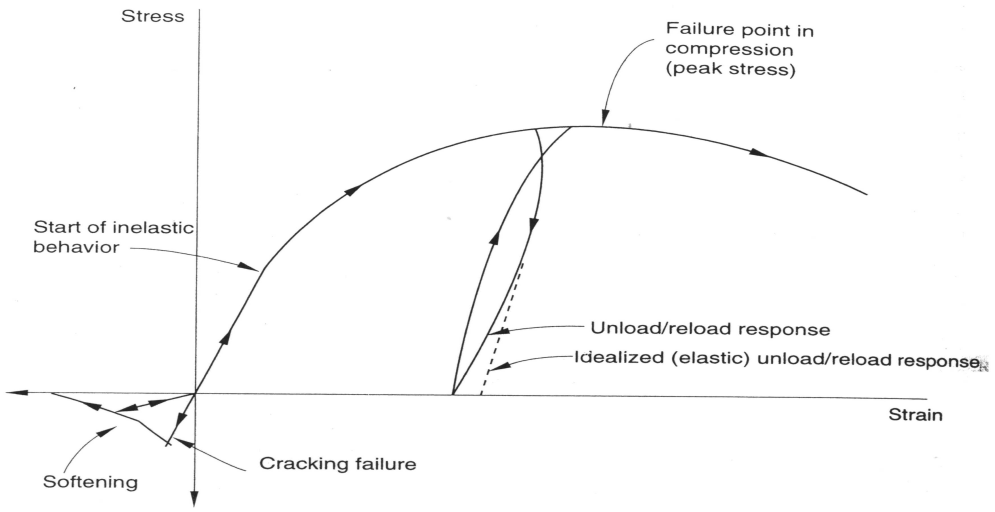

Figure 3.2. Uniaxial behaviour of plain concrete (ABAQUS Theory Manual 1998).

In the ABAQUS/Explicit program the brittle cracking model provides the capability to model tensile properties of concrete. This model is designated for applications in which the behaviour is dominated by tensile cracking. ABAQUS/Explicit uses a smeared crack model. A simple Rankine criterion is used to detect crack initiation. The Rankine criterion is presented in Fig. 3.3. A crack forms when the maximum principal tensile stress exceeds the tensile strength of the material. Further cracks of the same material point are orthogonal to any existing cracks (ABAQUS Theory Manual 1998).

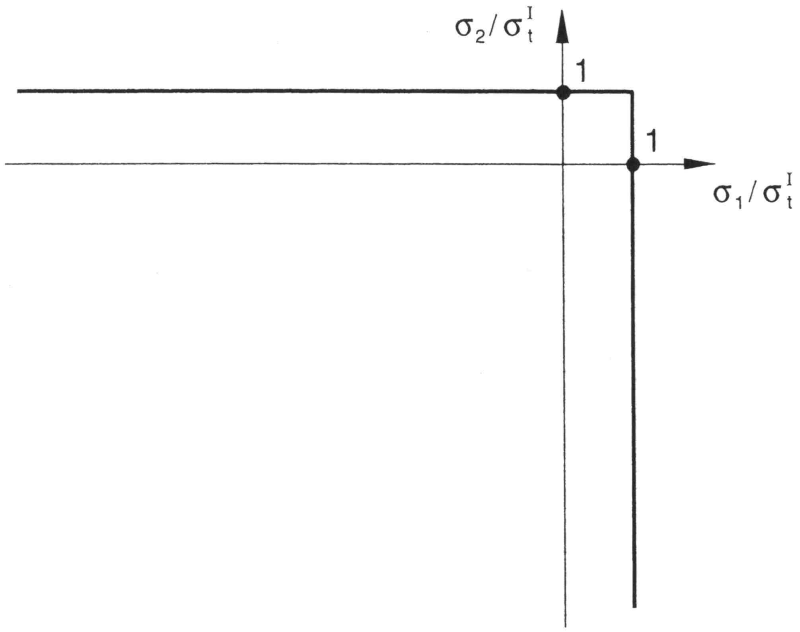

Figure 3.3. Rankine criterion in plane stress (ABAQUS Theory Manual 1998).

The crack forms when the maximum principal tensile stress exceeds the tensile strength of the concrete. A reasonable starting point for relatively heavily reinforced concrete modelled with a fairly detailed mesh is to assume that the tensile stress after failure linearly decreases when the strain ε_{tu} is ten times the strain at failure. In this case the strain at zero tensile stress is evaluated according to Shayanfar et al. (1997):

$$\varepsilon_{tu} = 0.004e^{-0.2h} \tag{3.1}$$

where h is the width of the element in inches. In this case h is about 4 inches.

The material properties of the concrete used in these non-linear analyses are shown in Table 3.1. The numerical values are obtained from codes and standards.

Table 3.1. Concrete material properties.

E_c [MPa]	f_{ctk} [MPa]	υ	ε_{cr}	ε_{tu}	f_{cd} [MPa]	f_{ck} [MPa]
27000	1.93	0.15	0.0007	0.0018	15.6	21

The mode II shear behaviour is based on the observation that shear behaviour depends on the amount of crack opening. The shear modulus decreases as the crack opens. Compressive behaviour is assumed to be linear elastic.

Standard material tests are conducted quasi-statically using a strain rate of 10^{-6} to 10^{-5} per second. Experiments simulating dynamic loading conditions with strain rates up to 0.2 per second show an increase in compression strength up to 35% when the strain rate increases. The increase in tensile strength by increasing strain rates is up to 50%. These rate-dependent properties of concrete cannot be numerically simulated with the available material model library.

Damping

Damping is modelled by the mass proportional part of Rayleigh damping; the damping matrix C is defined by

$$C = \alpha_R M + \beta_R K \tag{3.2}$$

where K is the stiffness matrix and M is the mass matrix. The α_R factor introduces damping forces caused by absolute velocities of the model and defines mass proportional damping. The factor β_R defines viscous material damping (Bathe & Wilson 1976).

Mass proportional damping is used to damp out the low frequency response. In this case the mass proportional damping is used for damping the lowest mode with 10% of the critical damping. The damping factor is calculated by

$$\alpha_R = 2\omega_{\min}\xi \tag{3.3}$$

where ξ in this study is basically 10%.

Reinforcement

Reinforcement is modelled by one-dimensional strain theory elements. Reinforcement is defined as layers of uniformly spaced reinforcing bars in shell elements. The concrete cracking is considered independently of rebars. Effects between concrete and the rebar interface, such as bond and dowel action, are modelled approximately by introducing some tension stiffening into the concrete cracking model. This simulates the load transfer across the cracks through the reinforcement.

The material behaviour of reinforcing steel is assumed to be linear elastic up to the yield stress. The stress vs. plastic strain is presented in Table 3.2. Young's modulus is 210 GPa and Poisson's ratio 0.3.

Table 3.2. Stress vs. plastic strain values for reinforcement steel.

Stress [MPa]	390.	400.	480.
Plastic strain [mm/mm]	0.	0.002	0.15

The strain rate effect of reinforcing steel is accounted for by a standard procedure for considering the strain rate effects, and is expressed by the formula

$$\dot{\varepsilon}_{pl} = D[\frac{\tilde{\sigma}}{\sigma_y} - 1]^p \tag{3.4}$$

where $\dot{\varepsilon}_{pl}$ is the equivalent plastic strain rate, $\tilde{\sigma}$ is the effective yield stress and σ_y is the static yield stress, ABAQUS/Explicit 5.8. In these calculations p = 5 and D = 40.

3.2 Loading transients due to hydrogen detonation

Pressure loading transients on the wall due to a hydrogen detonation are calculated by the DETO program (Silde & Lindholm 2000). The code is based on the strong explosion theory with oblique (and normal) shock reflection relations. Actually, the code models the adiabatic shock wave induced by point-like energy release. Propagation of the real detonation (combustion) front is not modelled. In any case, the code is found to yield the first, rough estimates of shock pressure loads typical in detonation conditions. Loading transients for the ABAQUS input file were produced by a special interface program. This interface program between the DETO code and ABAQUS Finite element code is described elsewhere (Silde 1999).

Shock pressure loads corresponding to the energy release from a burn of 0.5 kg hydrogen are shown in Fig. 3.4a. The explosion centre is 1.3 m away from the wall at the symmetry line of the model. The heights of the two ignition points considered are shown in Fig. 2.2. In the following, the ignition near the upper edge of the wall (level + 28.00 m) is referred to as Case 1.

Shock pressure loads corresponding to the energy release from a burn of 1.428 kg hydrogen are shown in Fig. 3.4b. The explosion centre is 1.3 m away from the wall. This corresponds to the situation referred to as Case 1 in Table 6-1 of the NKS Report (Silde & Lindholm 2000). Two different parameter variations were used: ignition near the upper location (Case 2) and in the lower location of the wall (Case 3). Ignition occurring in the upper position is referred to as Case 2 and detonation occurring at the level 21.50 as Case 3.

The over-pressure increases statically before detonation until 0.27 bar, and the constant over-pressure after detonation is 1.5 bar. According to the preliminary studies this clearly exceeds the ultimate capacity of the wall.

The numerical simulations were carried out in three steps. The time increment needed for explicit time integration was 5 μs. First, the constant loading pressure on the non-linear part of the model was increased to 0.27 bar in 0.1 seconds. During the second step the detonation transient was applied to the wall. The duration of this step was 3.5 ms. Constant pressure during the final step was 1.5 bar.

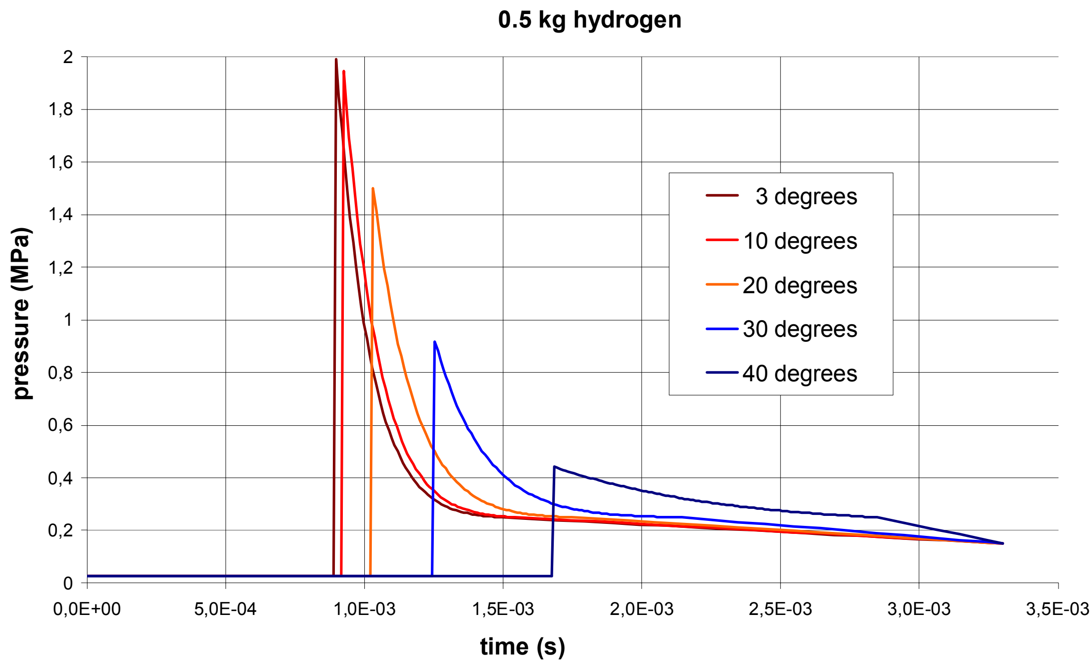

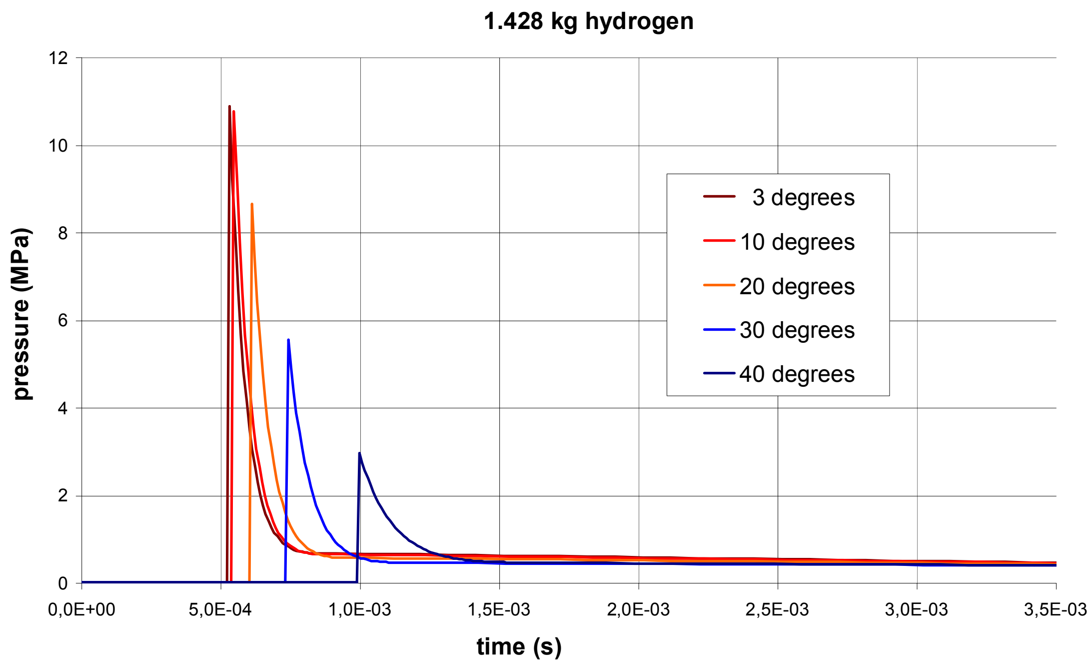

Figure 3.4 a and b. Pressure transients on the wall during detonation transients of 0.5 kg and 1.428 kg hydrogen.

Decrease of the constant over-pressure after detonation due to ventilation has also been assessed (Lindholm 2000). The initial temperature in room B.60-80 is assumed to be 800 K and in the outer room 303 K, respectively. The pressure in the outer room is assumed as 1 bar.

In the first scenario the joint sealing compound is absent and the area of the ventilation hole is 0.67 m^2. Pressure decrease as a function of time with different initial pressure differences is shown in Fig. 3.5. The pressure decrease rate is rather low and does not affect the constant pressure load as rapidly as needed in respect of the wall point.

In the second scenario the doors at level 19.00 are assumed to be open in addition to the hole in the seam area. The ventilation hole is 4.67 m^2. In this case the pressure decrease affects the constant pressure load significantly. The pressure decrease is shown in Fig. 3.6 in a case where the initial pressure difference is 2 bar.

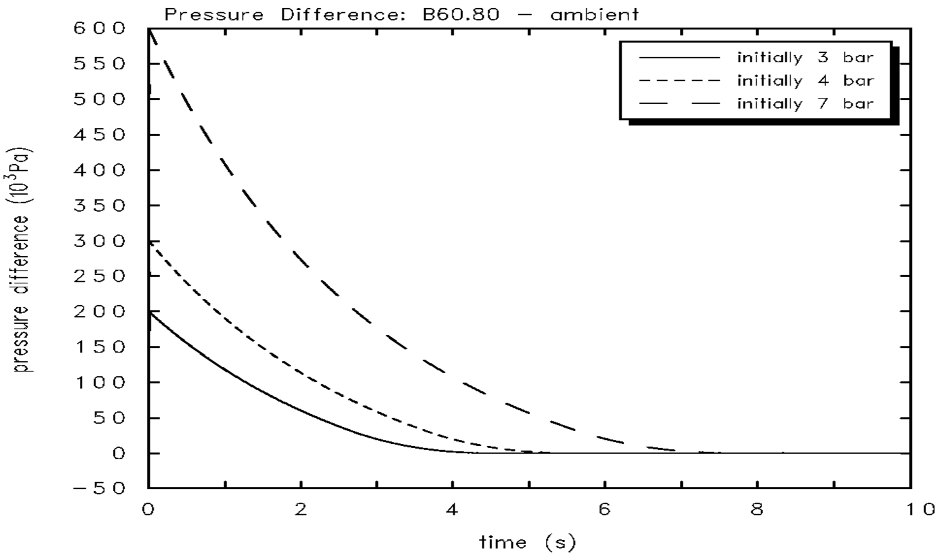

Figure 3.5. Pressure increase at different pressure differences, hole 0.67m^2.

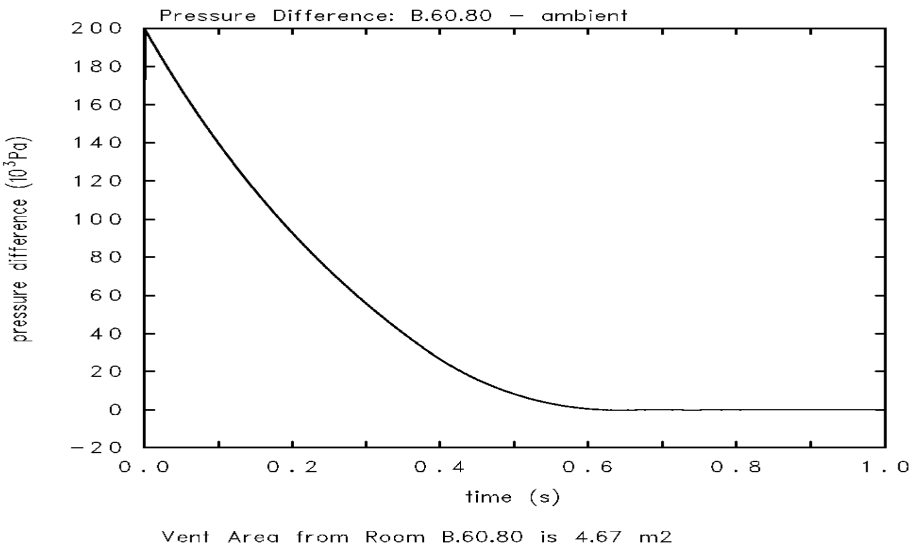

Figure 3.6. Pressure increase at different pressure differences, hole 4.67 m^2.

4 Results

In non-linear studies only model of the wall was used. For conservative reasons the supporting structures were modelled by simplified boundary conditions described in the end of the chapter 2. Shell element used in these calculations is called S4R in ABAQUS/Explicit program. It is a 4-node doubly curved shell element with hourglass control and finite membrane strains.

4.1 Constant load

The non-linear element model was first loaded with a constant pressure. These analyses were carried out with the ABAQUS/Standard using the Riks method for the proportional loading procedure, and with the ABAQUS/Explicit program increasing the load gradually.

The material properties presented in Chapter 3.1 were applied. Only the zero tensile strain value was varied. Values of $1.8*10^{-3}$, $0.9*10^{-3}$ and $1.8*10^{-2}$ were used in static ABAQUS/Standard analyses. The first value is calculated according to Equation (3.1). The second value is obtained by dividing the first calculated value by 2, and is equal to 12.6 times the cracking strain, which is close to the value of the cracking strain multiplied by ten. In the following these are referred to as Cases A, B and C, respectively.

Dynamic ABAQUS/Explicit analyses were carried out using the zero tensile value of $1.8*10^{-3}$ and varying the load increasing rate. In Case D the load increasing rate was 3 bar/s, in Case E the pressure load was increased by 1.4 bar/s and in Case F the load increase rate was 0.7 bar/s.

Pressure loads as a function of the deflection of the upper edge of the model, at the symmetry line, are presented in Fig. 4.1. The results of these analyses may be treated as reliable until the energy balance holds reasonably, which in this case means a deviation of less than 10% of the total energy. In Cases A-C the energy balance is lost when the pressure exceeds 0.4 bar. In Cases D-F the energy balance holds until the pressure exceeds 0.6 bar. The ultimate capacity of the wall seems to be somewhere beyond 0.5 bar. Also, the concrete is no longer behaving elastically in the compressed part of these cross-sections. Pressure values at reinforcement yielding and concrete compression crushing are summarised in Table 4.1. The parameters varied in these analyses are summarised in the first row.

Table 4.1. Summary of predicted pressure values [bar].

Case	A $\varepsilon_{tu} = 1.8*10^{-3}$		B $\varepsilon_{tu} = 0.9*10^{-3}$		C $\varepsilon_{tu} = 1.8*10^{-2}$		D rate 3 bar/s $\varepsilon_{tu} = 1.8*10^{-3}$		E rate 1.4 bar/s $\varepsilon_{tu} = 1.8*10^{-3}$		F rate 0.7 bar/s $\varepsilon_{tu} = 1.8*10^{-3}$	
Region	1	3	1	3	1	3	1	3	1	3	1	3
Reinf. yielding	0.73	0.55	0.65	0.4	0.8	0.8	0.8	0.5	-	0.5	-	0.4
Concrete comp. crush	0.55	0.55	0.5	0.4	0.55	0.8	0.5	0.7	0.5	0.5	0.5	0.6

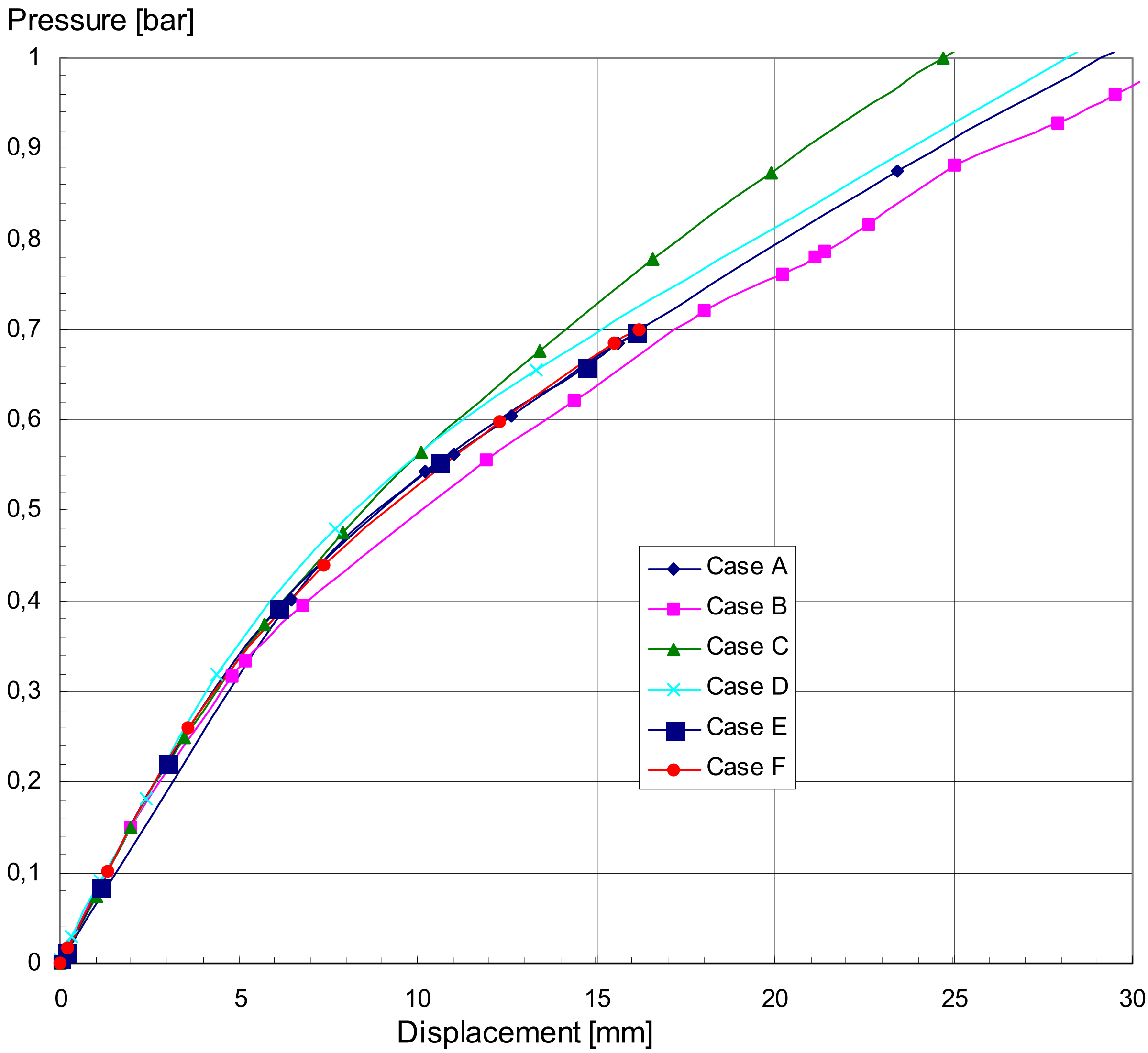

Figure 4.1. Pressure loads as a function of maximum displacement.

4.2 Decreasing pressure

According to the preliminary calculations, the wall does not resist well a constant static overpressure exceeding 0.5 bar. After a detonation, the static pressure may be relatively high. After a 0.5 kg hydrogen detonation the static type pressure is 1.5 bar. Thus this kind of static pressure may damage the wall severely even if it has survived a detonation peak. The effect of the pressure decrease following the detonation transient has also been studied. According to Fig 3.6, the pressure after detonation of 0.5 kg hydrogen as shown in Fig. 3.4a decreases to zero in 0.5 seconds if the ventilation hole is 4.67 m^2, and in 2.0 seconds if the ventilation hole is 0.67 m^2 (Fig. 3.5).

Dynamic non-linear analyses were performed by the ABAQUS/Explicit program, which is based upon implementation of an explicit integration rule together with the use of diagonal element mass matrices. The equations of motion are integrated using the explicit central difference integration rule.

Structural analyses were carried out to find a relatively slow linearly decreasing pressure loading which the wall resists. The peak value of this triangular shape loading was decreased to 0.5 bar and the duration to 0.25 seconds.

Dynamic magnitification factor

The maximum undamped response of a SDOF (Single Degree Of Freedom) system which is subjected to a shock motion depends on the ratio of the impulse duration (t_l) to the natural period of the vibration system (T), i.e. t_l/T (Boswell & D'Mello 1993) as shown in Fig. 4.2.

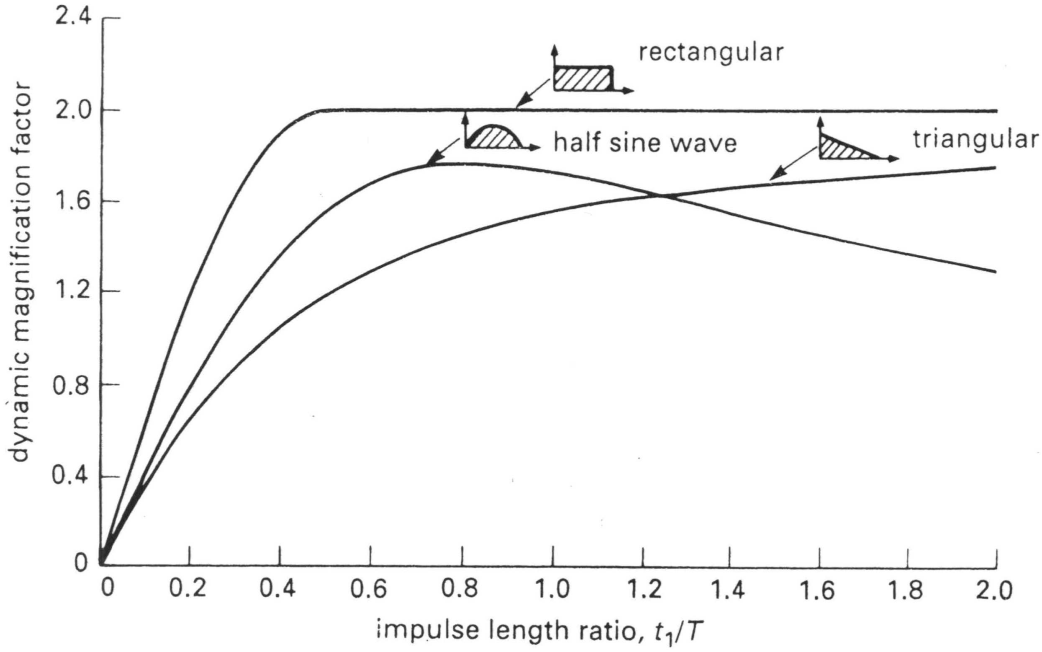

Figure 4.2. Dynamic magnification factor as a function of impulse length ratio (Boswell & D'Mello 1993).

The dynamic magnification factor for a triangular-shaped pulse increases monotonically and reaches 1.8 at an impulse length ratio of 2.

The first eigenfrequency of the wall model is 14.5 Hz (see Table 2.1) and the duration T_l of the first eigenperiod in this case is 69 ms. The impulse length ratio is 3.6. Thus it can be expected that the effect of the decreasing type pressure load has a magnification factor greater than one, compared to the effect of the static pressure load.

If the duration of the pulse is markedly shorter than the period of vibration, the impact factor is less than one. The structure can resist dynamic loads with relative high peak values provided the duration is short. For a detonation peak load the impulse length ratio may be e.g. 0.01. These speculations are only qualitative. The problem tackled in this study is far more complex than an undamped SDOF system.

The energy balance during a pressure decrease in 0.25 s and the following 0.25 s is shown in Fig. 4.3. The external work done by the increasing load (ALLWK) creates kinetic energy (ALLKE), strain energy (ALLIE) and part of the external work is dissipated by viscous effects (ALLVD) like damping. The total strain energy further consists of recoverable strain energy (ALLSE) and energy transfer to plastic deformations (ALLPD). ETOTAL shows the total energy balance (ETOTAL=ALLKE+ALLIE+ALLVD-ALLWK). The ETOTAL value is zero if the energy balance holds. So far, the total energy balance is negligible, thus a difference of about 5% of the energy due to the external work is acceptable, and the results are reliable from the energy balance point of view. In this case the difference in energy balance is about 10% but remains constant.

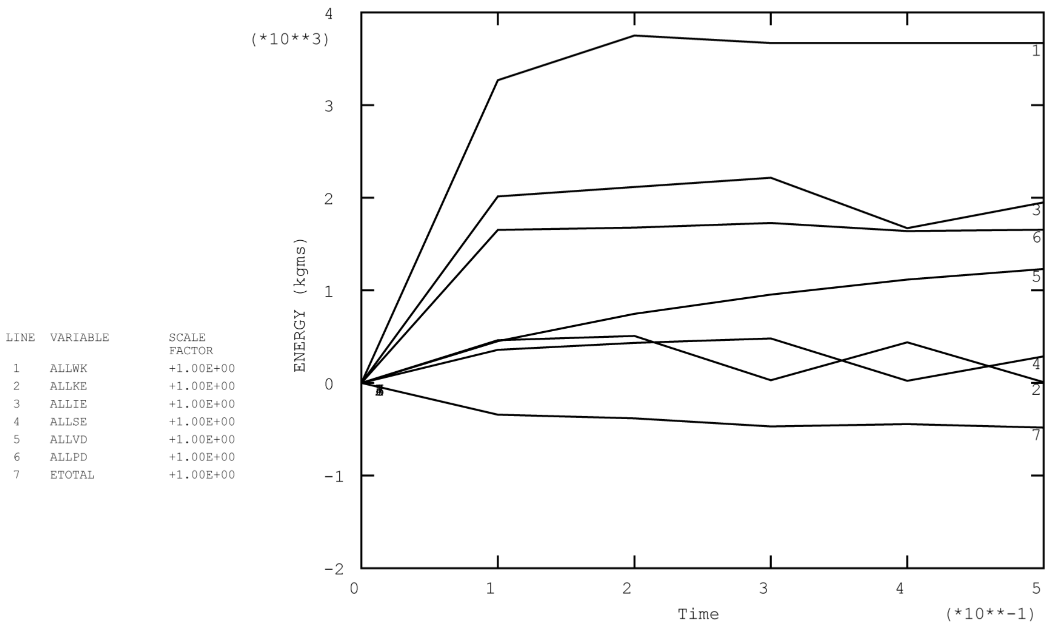

Figure 4.3. Energy balance, unified 0.5 MPa pressure decreasing linearly in 0.25 seconds.

The total energy dissipated per unit volume in the element by rate-independent and rate-dependent plastic deformation in presented in Fig 4.4, at the end of the calculation t = 0.5 s.

The cracks on both sides of the wall and in the middle of the wall are shown in Figs 4.5 a-c at t = 0.5 s. On the outer surface, the cracks are mainly located in the field area (Fig. 4.5 a). In contrast, at the inner surface the cracks are located near the support area (Fig. 4.5 c). The lower part of the wall remains uncracked in the middle of the wall (Fig. 4.5 b).

Cracking is extensive near the supporting wall and floor areas. The compressive strength of the concrete is not exceeded.

The reinforcement yields in the area of highest dissipated plastic energy density, as seen in Fig. 4.4. The vertical reinforcement at the supporting floor (level 25.00) near the inner surface of the wall is yielding. Development of plastic deformation in the reinforcement at the symmetry line and at locations 0.5 m, 1.0 m and 1.5 m away from the symmetry line along floor level 25.00 is shown as a function of time in Fig. 4.6. Plastic strains are relatively low and do not increase once the pressure reaches zero.

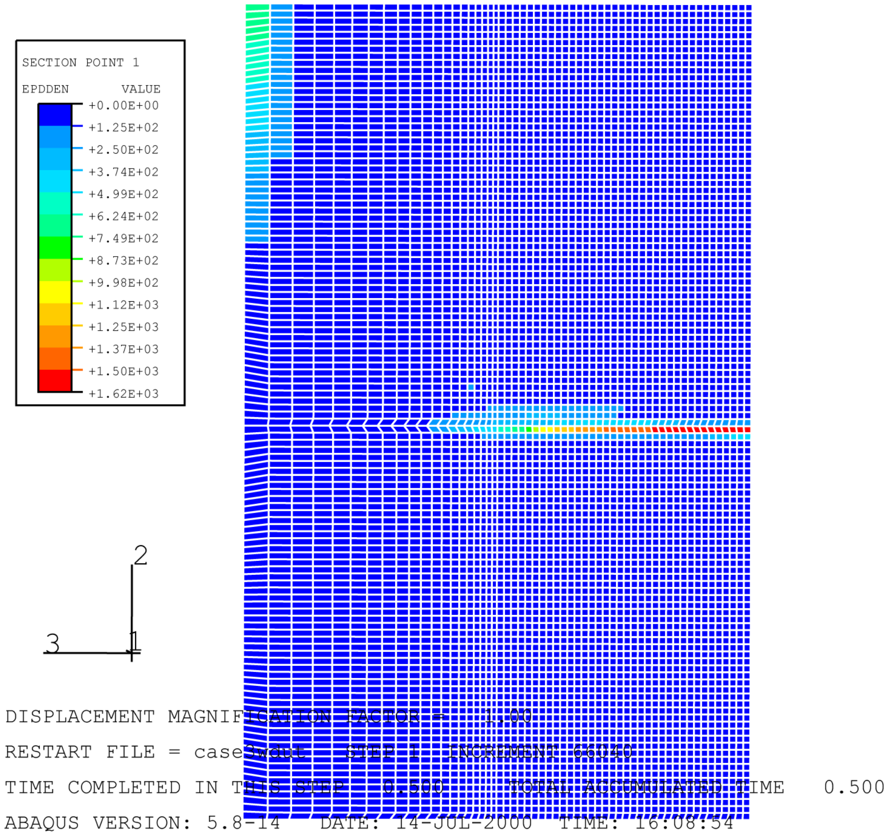

Figure 4.4. Plastic deformation energy dissipated per unit volume, t = 0.5 sec.

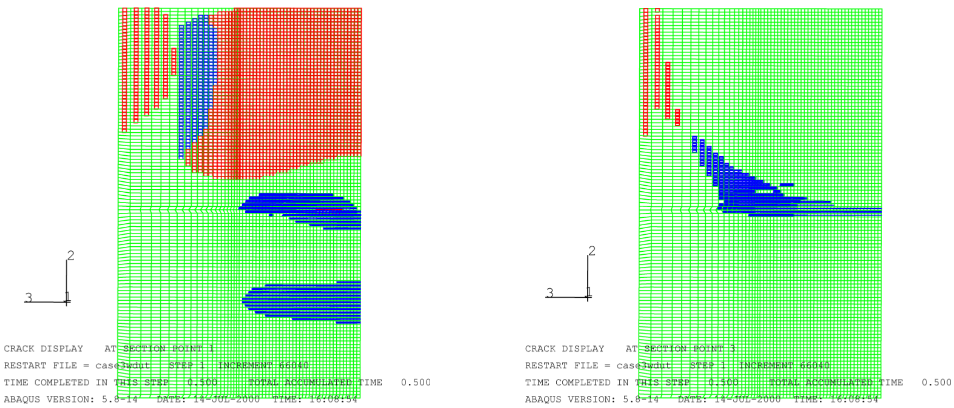

Figure 4.5 a. Crack distribution at the outer surface, b) in the middle of the wall t = 0.5 sec.

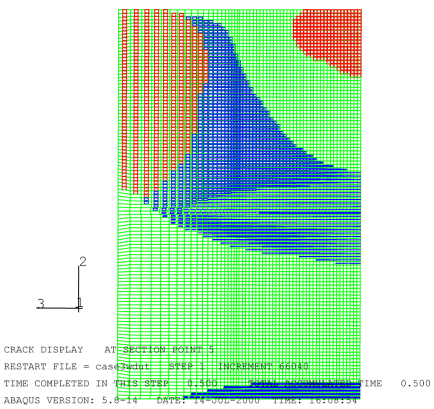

Figure 4.5 c. Crack distribution at the inner surface, t = 0.5 sec.

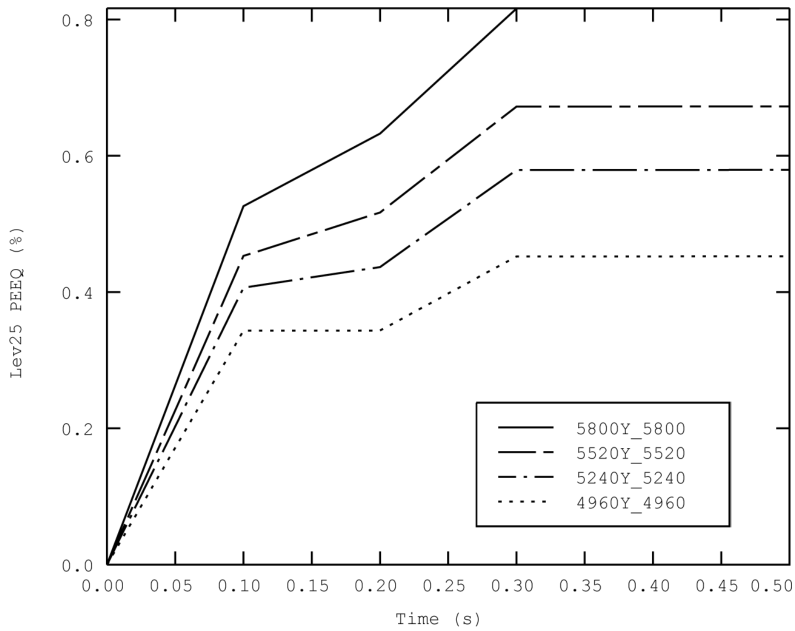

Figure 4.6. Plastic deformation of reinforcement at the support, level 25.00.

Because this kind of pressure impact already seems to damage the wall severely, in the following the pressures after the detonations are assumed to be lower that the calculated pressure values after detonation.

According to previous studies, slowly decreasing pressure after detonation seems to destroy the wall. After the detonation peak the structure is less stiff due to cracking, and also the duration of the eigenperiod is longer. Accordingly the magnification factor would in this case be lower. Due to damping and non-linear effects, the above speculation based on the SDOF system has only a qualitatively sense.

4.3 Detonation transients

In these studies the detonation is assumed to occur at the symmetry line of the model. The 'upper'place definition means 3 meters below the upper edge of the wall. 'Lower' means 2.5 meters above the lower edge. First, three detonation cases after which the pressure fell to zero in 0.25 seconds were considered. This triangular shaped pressure load is described in the previous chapter.

The effects of several parameters were studied upon 0.5 kg of hydrogen detonating near the top of the wall. These studies are referred to in the following as Cases 1a, 1b, 1c and 1d. A summary of these cases is presented in Table 4.2.

Table 4.2. Summary of the studied cases.

Case	Hydrogen [kg]	Place	Damping	ε_{tu}	Strain rate effect D, p	Degr. time [sec]
1a	0.5	upper	10%	$1.8*10^{-2}$	40, 5	0.25
1b	0.5	upper	no	$1.8*10^{-2}$	40, 5	0.25
1c	0.5	upper	10%	$1.8*10^{-3}$	40, 5	0.25
1d	0.5	upper	10%	$1.8*10^{-3}$	40, 5	0.5
2	1.428	upper	10%	$1.8*10^{-3}$	40, 5	det. only
3	1.428	lower	10%	$1.8*10^{-3}$	40, 5	det. only

4.3.1 Case 1

According to Table 4.2, in Cases 1a, 1b, 1c and 1d a detonation corresponding to 0.5 kg of hydrogen was assumed to occur in the upper part of the wall. The pressure increase up to 0.27 bar is assumed to occur in 0.1 seconds before detonation. The duration of the detonation is 3.5 ms. After the detonation the pressure decreases from 0.5 bars to zero in 0.25 seconds or in 0.5 seconds and there is no pressure during the last time period of the numerical simulation. In Cases 1a-1c the behaviour of the wall is simulated during 0.604 seconds starting from the pressure increase before detonation. The initial time increment used in these analyses was 7.5 μs and about 66 000 increments were needed for this calculation.

One calculation was carried out using the pressure value of 0.75 bar after detonation, decreasing to zero in 0.25 s. Due to the loss of energy balance the results are not reliable and not worth presenting here.

Case 1a

In Case 1a the Rayleigh damping corresponding to 10% of the critical damping and the strain rate effect on the yield strength of the reinforcement were taken into account. The tensile stress was assumed to decrease to zero unrealistically slowly ($\varepsilon_{tu} = 1.8*10^{-2}$) in order to get results for damping parameter studies. The energy balance during the loading transient is shown in Fig. 4.7. The kinetic energy drops nearly to zero towards the end of the simulation, mainly due to damping and inelastic effects.

The same phenomena can be seen in Fig. 4.8, where displacements in locations normal to the wall in two locations at the symmetry line are shown as a function of time. Notation Deto refers to the point located in the area where the detonation first hits the wall. Notation Lev31sl refers to the nodal point located at the symmetry line and on top of the wall. As can be seen, the wall hardly moves at all during the detonation peak. Because the upper edge of the model is totally free, the maximum displacement occurs in this corner (Fig. 4.7) in the curve referred to as Lev31sl.

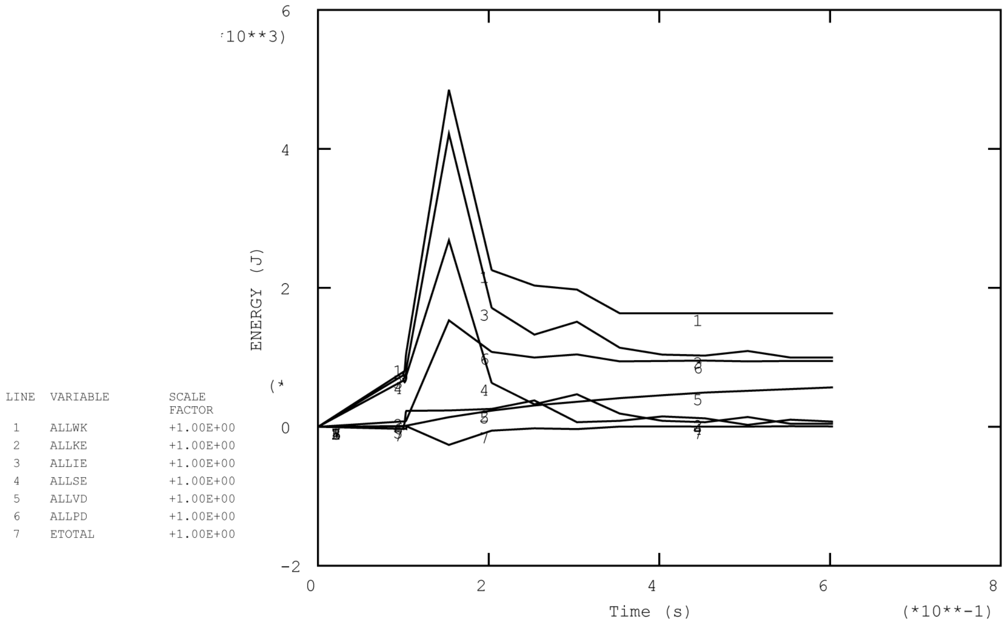

Figure 4.7. Energy balance as a function of time, Case 1a.

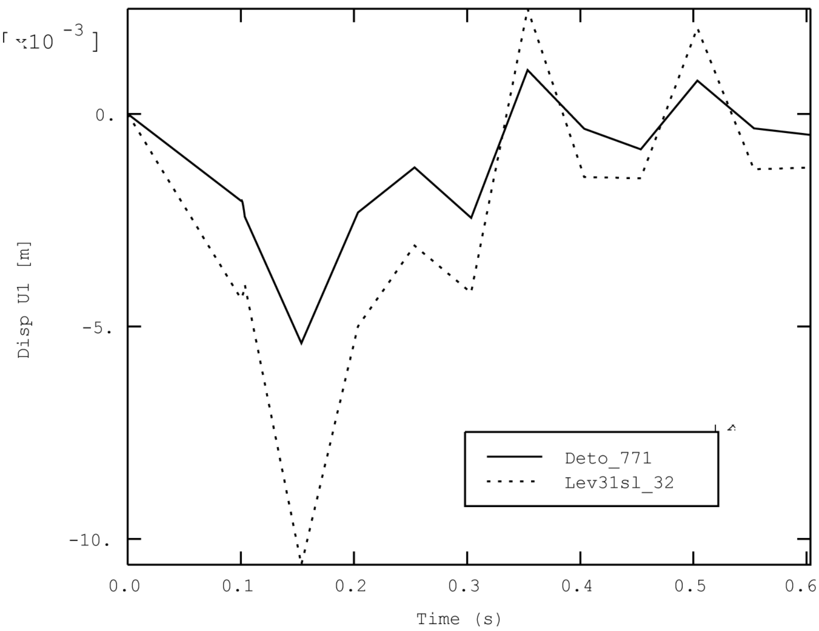

Figure 4.8. Displacements at the symmetry line as a function at time, Case 1a.

Bending moment distributions after the pressure increase just before detonation are shown in Figs 4.9 and 4.10.

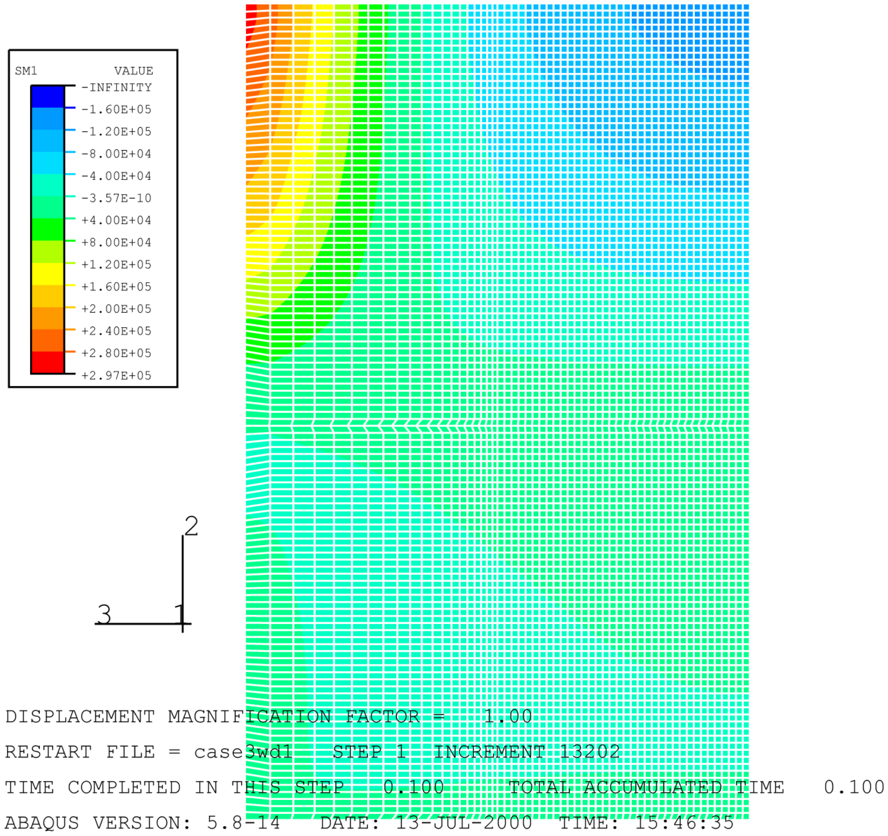

Figure 4.9. Bending moment SM1 distribution [Nm] after the pressure increase, Case 1a.

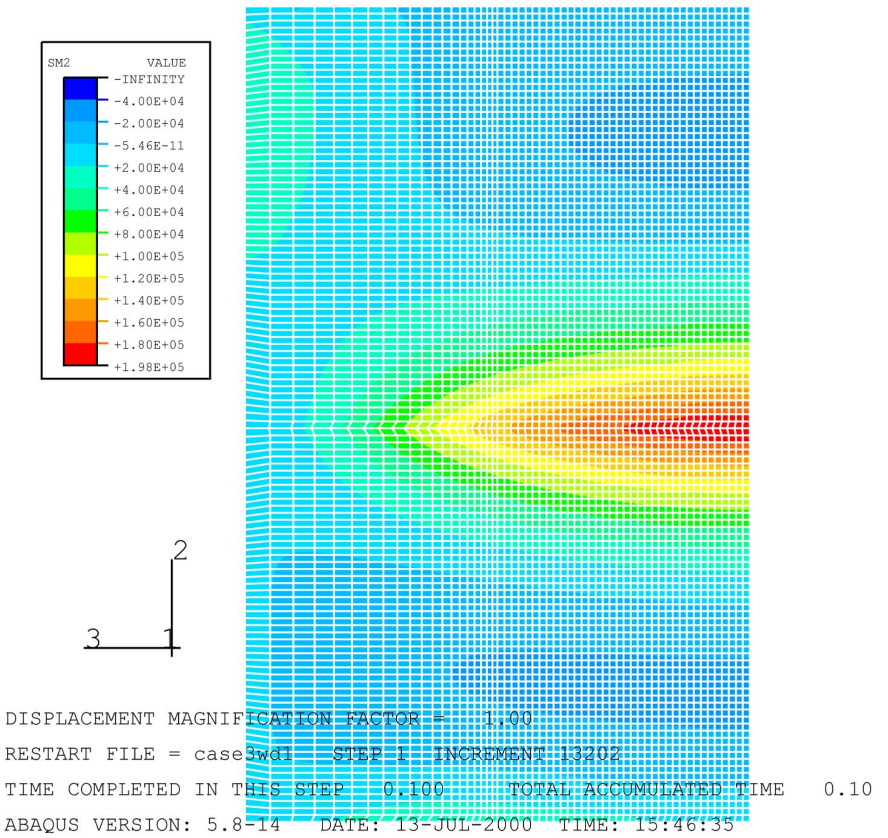

Figure 4.10. Bending moment SM2 distribution [Nm] after the pressure increase, Case 1a.

Development of cracks at the outer and inner surfaces of the wall are shown in Figs 4.11 a-h. The surface loaded by the pressure is referred to as the inner surface. Cracking on the outer and inner surfaces after the pressure increase and just before the detonation peak are shown in Fig. 4.11 a and b. The outer surface is cracked near the corner of the model, where the symmetry line meets the upper edge.

Cracking occurs in the supporting areas at the inner surface, i.e. near the wall at the left edge of the model and near the floor at level 25.00. The left edge of the model is modelled as fully fixed, simulating the supporting effects due to surrounding structures. The boundary condition due to the floor is modelled as simply supported. The displacements normal to the wall are fixed along level 25.0. The lower edge of the model is fully fixed.

Crack propagation at the outer surface of the wall during the detonation transient is shown in Figs 4.11 c, e and g. Cracking near the supporting areas is shown in Figs 4.11 d, f and h.

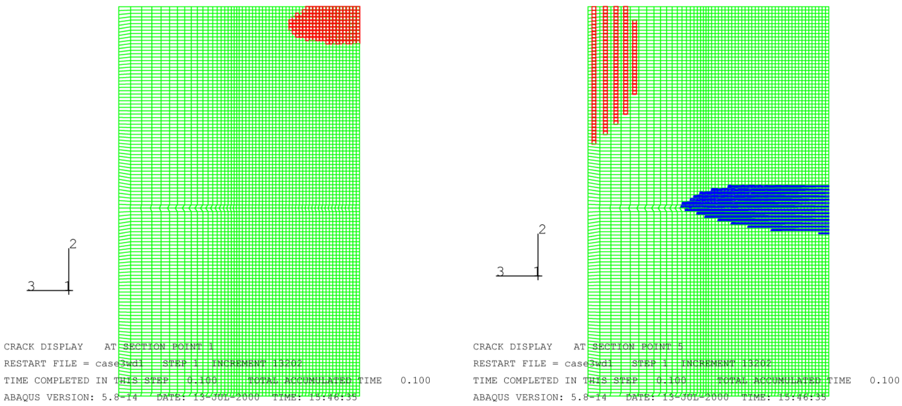

Figure 4.11 a, b. Cracks at the outer (a) and inner (b) surfaces before detonation, t = 0.1 s, Case 1a.

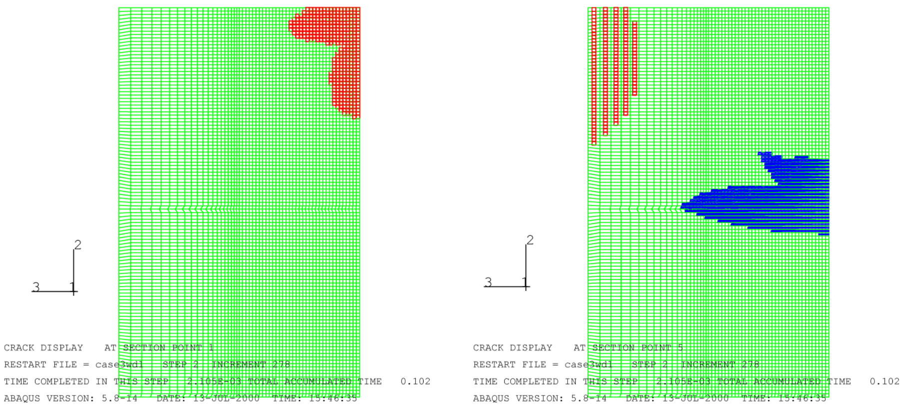

Figure 4.11 c, d. Cracks at the outer (c) and inner (d) surfaces, t=1.02 s, Case 1a.

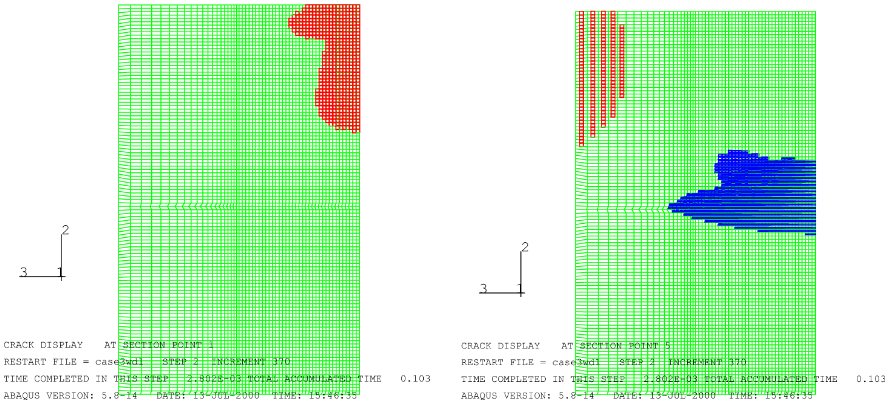

Figure 4.11 e, f. Cracks at the outer (e) and inner (f) surfaces, t=1.03 s, Case 1a.

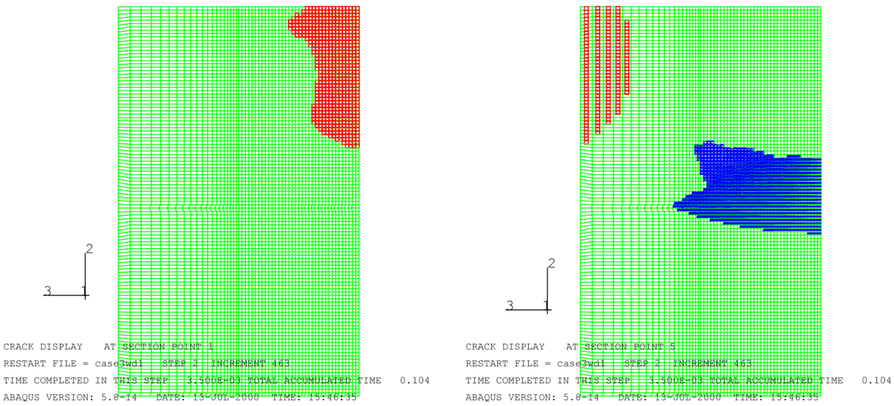

Figure 4.11 g, h. Cracks at the outer (g) and inner (h) surfaces, t = 1.04 s, Case 1a.

Cracks at the end of the calculation are shown in Figs 4.12 a and b, Case 1a.

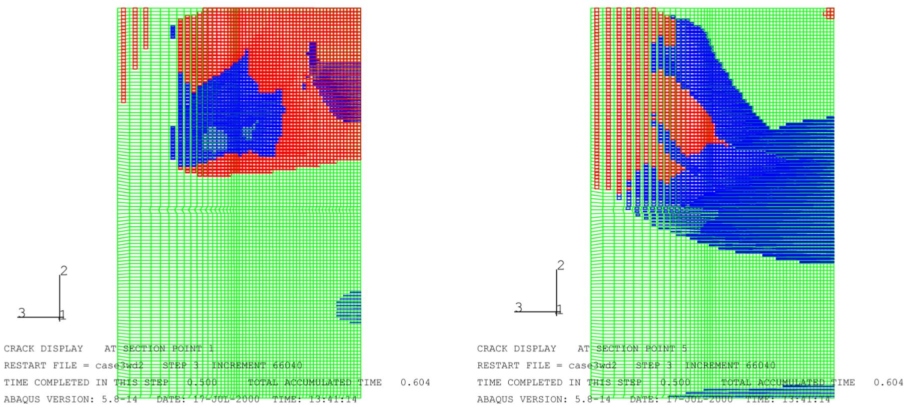

Figure 4.12 a, b. Cracks at the outer (a) and inner (b) surfaces at end of calculation, Case 1a.

The cracking strain magnitude is defined as

$$CKEMAG = \sqrt{\left(e_{nn}^{ck}\right)^2 + \left(e_{tt}^{ck}\right)^2 + \left(e_{ss}^{ck}\right)^2} \qquad (4.1)$$

where e^{ck}_{nn} e^{ck}_{tt} e^{ck}_{ss} are cracking strains. Contour plots of cracking strain magnitude distributions are shown in Figs 4.13 a-b. Because at the end of the calculation the model is slightly deformed outwards, the open cracks are at the outer surface near the symmetry line and at the inner surface near the supporting areas.

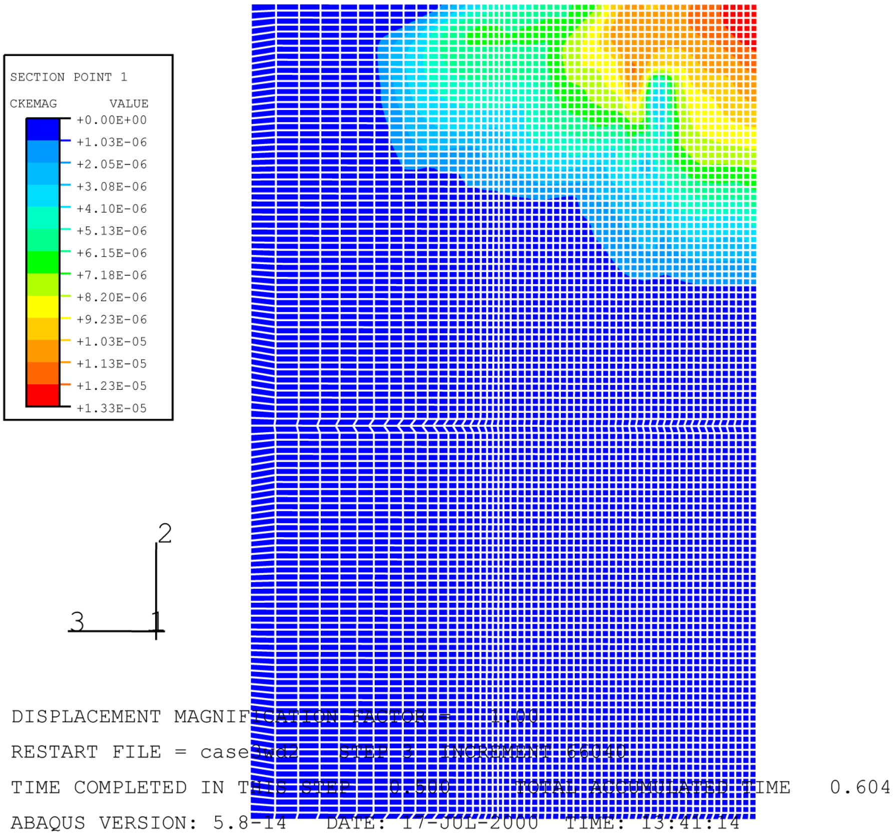

Figure 4.13 a. Cracking strain magnitude at the outer surface of the wall at end of calculation.

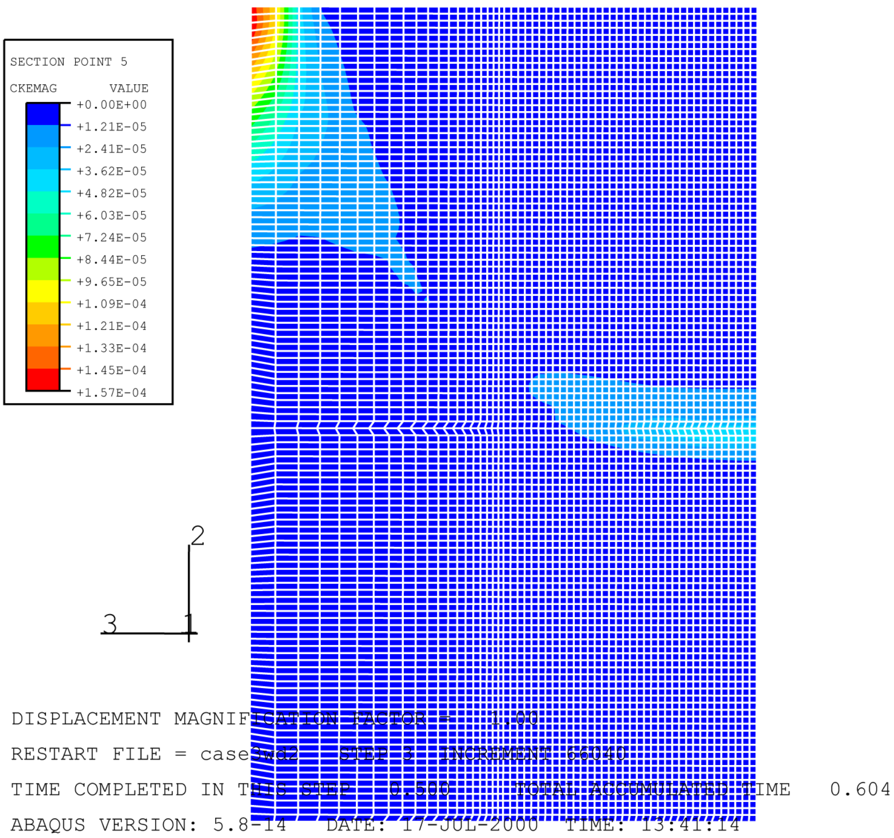

Figure 4.13 b. Cracking strain magnitude at the inner surface of the wall at end of calculation.

The cracking strain magnitude distribution reaches its maximum value on the outer surface, near the symmetry line. Crack strain magnitude contours at the end of the calculation, corresponding the cracking situation shown in Figs 4.12 a and b, are shown in Figs 4.13 a and b.

It should be noted that all the cracks, not only the open ones, are shown in Figs 4.12 a and b. The maximum crack strain is less than $2*10^{-5}$ near the symmetry line (Fig. 4.13 a). The corresponding value near the support area is less than $2*10^{-4}$ (Fig. 4.13 b).

Case 1b

Case1b looks at the effect of damping. The tensile stress was assumed to decrease to zero unrealistically slowly ($\varepsilon_{tu} = 1.8*10^{-2}$) in order to get results for damping parameter studies. The only difference from the previous case is that there is no damping involved. This phenomenon is also seen in the energy balance during the loading transient shown in Fig. 4.14.

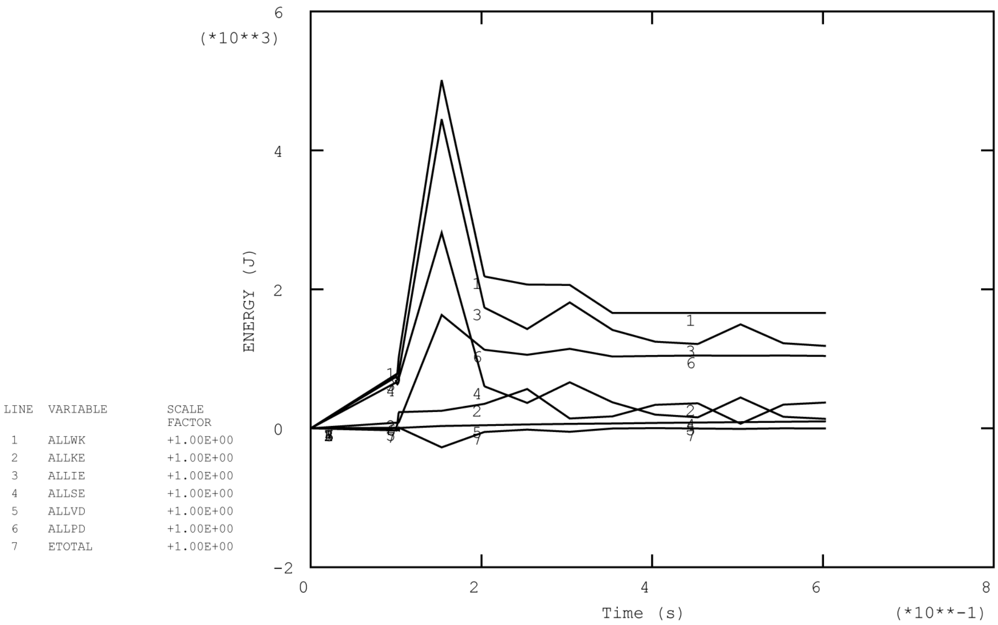

Figure 4.14. Energy balance as a function of time, Case1b.

The kinetic energy does not decrease as effectively as in the previous case, where damping was involved. The energy dissipated by the viscous effects stays at zero (Curve 5). Due to the slower decreasing kinetic energy, there is more cracking on both sides of the wall at the end of the calculation. The energy used for plastic deformations at the end of the calculation is slightly higher compared with the previous, damped case.

Crack propagation at the outer surface of the wall during and after the pressure increase, after the detonation peak transient and at the end of the calculation, are shown in Figs 4.15 a, c and e. Cracking of the inner surface is shown in Figs. 4.15. b, d and f.

The behaviours during the pressure increase before the detonation peak are fairly similar compared with Case 1a (Figs 4.11 a-b and Figs 4.15 a-b). Also the detonation occurs so rapidly that damping does not affect the results during the sharp detonation peak (Figs 4.11 g-h and Figs 4.15 c-d).

Due to the more slowly decreasing kinetic energy in the undamped case, there is more cracking on both sides of the wall at the end of the calculation (see Figs 4.12 a-b compared with Figs 4.15 e-f).

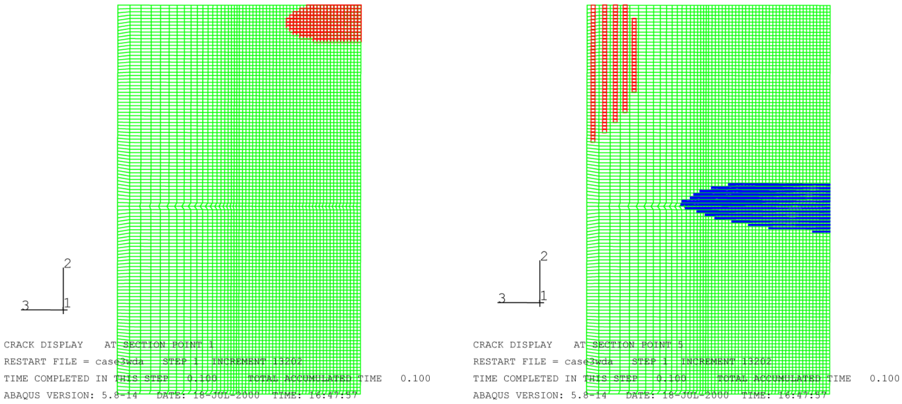

Figure 4.15. Cracks at the outer (a) and inner (b) surfaces, t = 0.1 s, Case 1b.

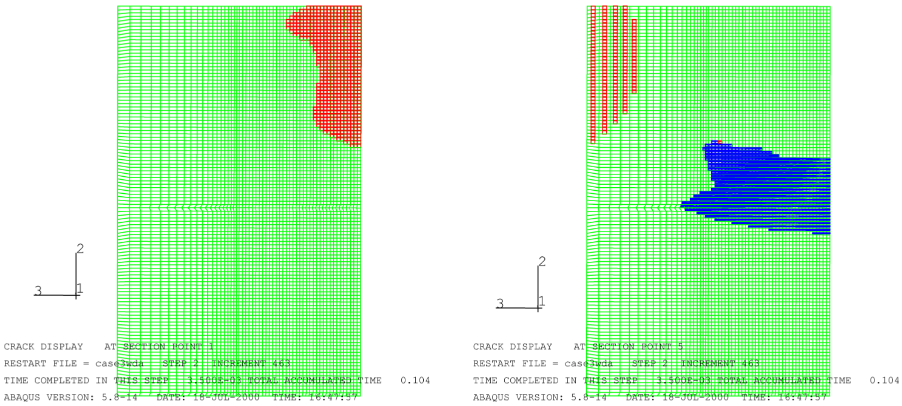

Figure 4.15. Cracks at the outer (c) and inner (d) surfaces, t = 0.104s, Case 1b.

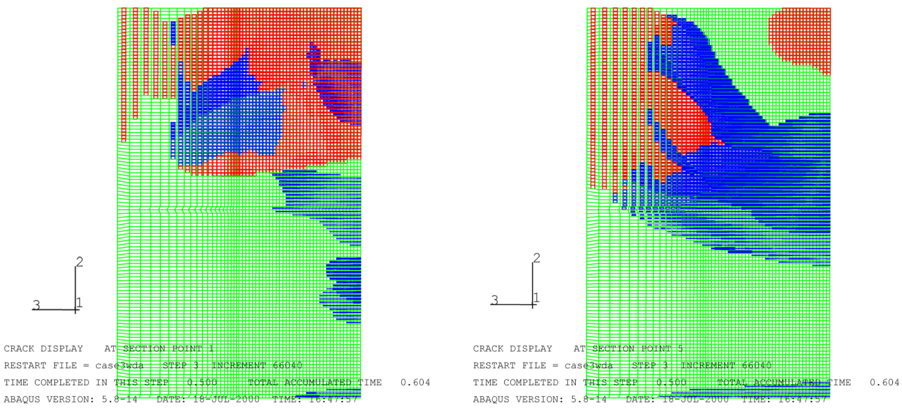

Figure 4.15. Cracks at the outer (e) and inner (f) surfaces, at end of calculation, Case 1b.

<u>Case 1c</u>

Case 1c looked at the effect of the cracking parameter ε_{tu}. The tensile stress was assumed to decrease to zero when $\varepsilon_{tu} = 1.8*10^{-3}$. This value was predicted in Chapter 3.1 according to the recommendations. The energy balance during the loading transient is shown in Fig. 4.16.

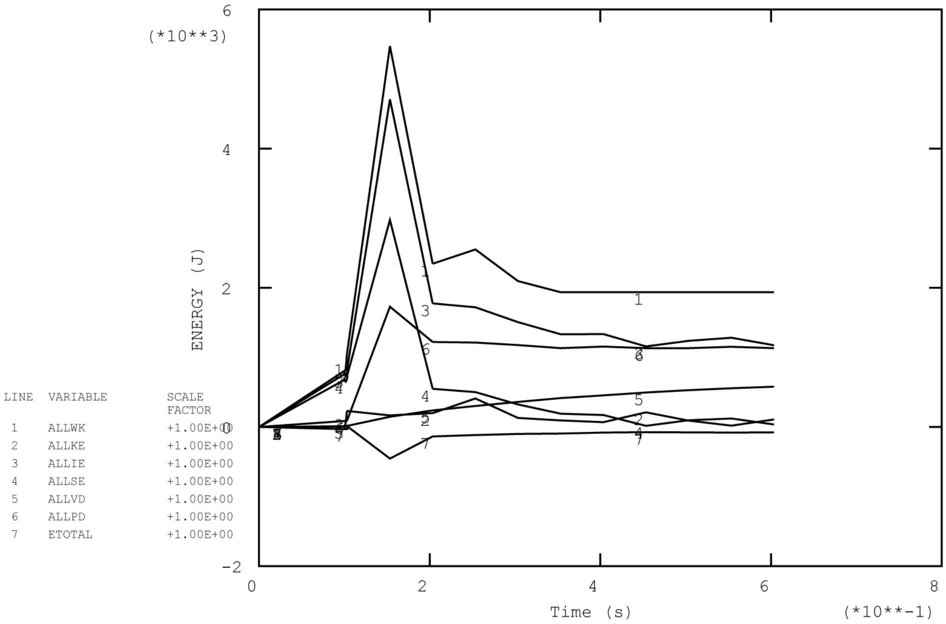

Figure 4.16. Energy balance as a function of time, Case 1c.

Total energy dissipated per unit volume in the element by rate-independent and rate-dependent plastic deformation is presented in Fig 4.17, at the end of the calculation t = 0.604 s. This distribution looks quite similar to that in Fig 4.4, where the corresponding plastic deformation energy dissipation is shown after the pressure decrease without any detonations. Also in Case 1c the reinforcement yields somewhat near the junction with the floor at level 25.00.

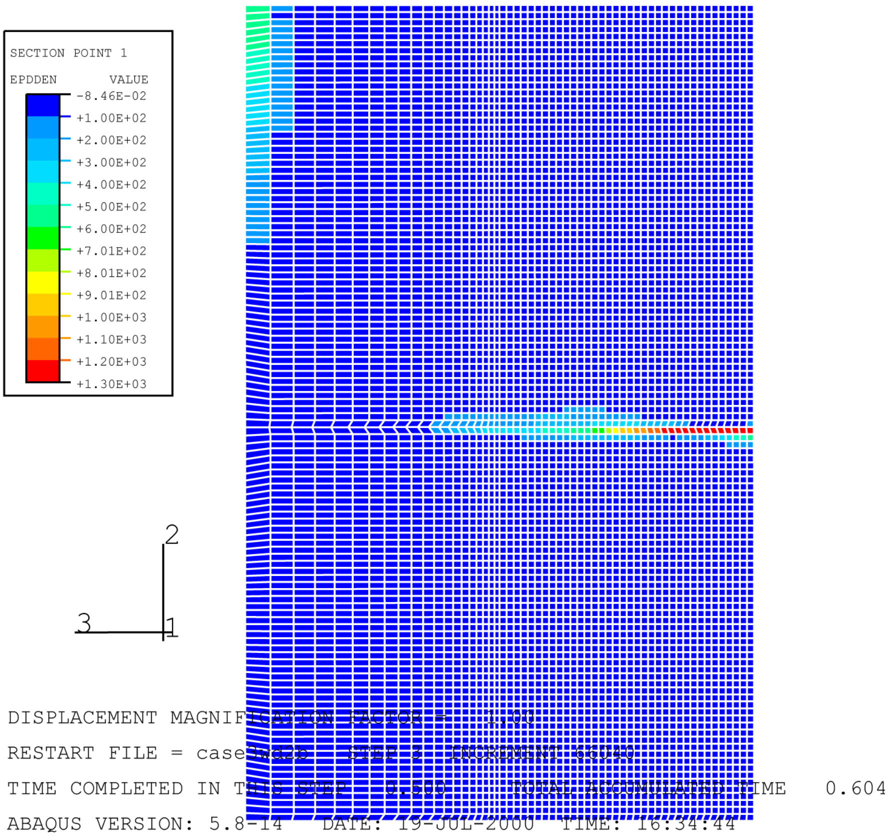

Figure 4.17. Total energy dissipated per unit volume by plastic deformation, Case 1c.

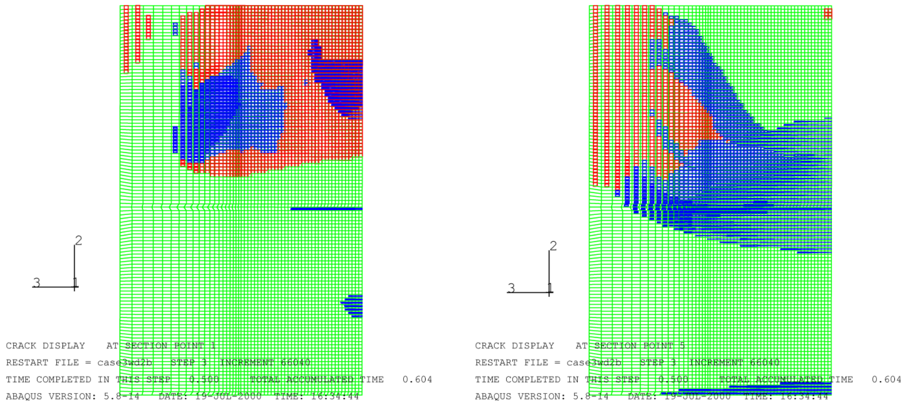

Figure 4.18. Cracks at the outer (a) and inner (b) surfaces at end of calculation, Case 1c.

Cracks at the outer and inner surface of the wall at the end of the calculation are shown in Figs 4.18 a and b. These crack distributions are almost equal to the corresponding distributions in Case 1a (Figs 4.12 a and b). There is cracking through the wall in the supporting floor area.

In Case 1c the reinforcement yields because the steel bars are carrying tensile stresses after cracking of the concrete sooner than in Case 1a, where the tensile stresses of the concrete were decreased to zero unrealistically slowly.

Case 1d

In Case 1d the effect of a static-type pressure decrease is studied. The tensile stress was assumed to decrease to zero when $\varepsilon_{tu} = 1.8*10^{-3}$. This value was predicted in Chapter 3.1 according to the recommendations. The energy balance during the loading transient is shown in Fig. 4.19.

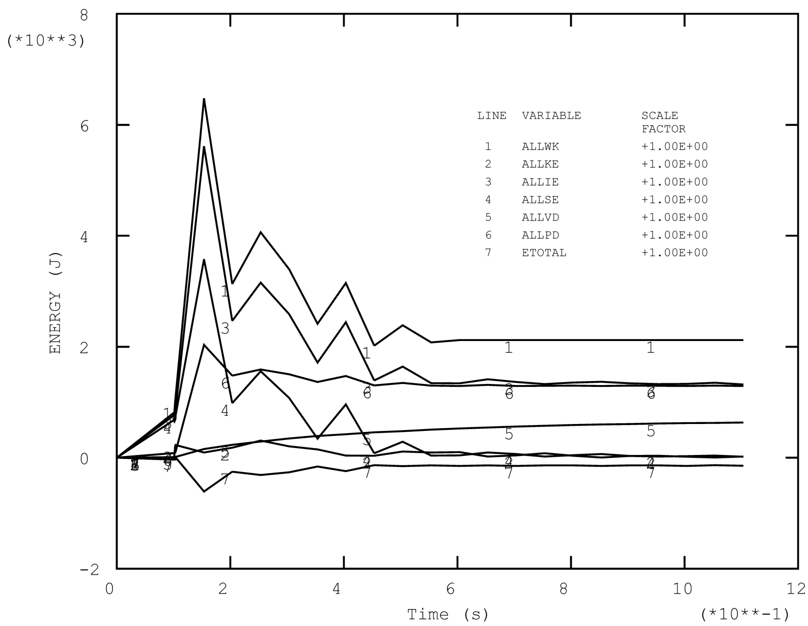

Figure 4.19. Energy balance as a function of time, Case 1d.

The total energy dissipated per unit volume in the element by rate-independent and rate-dependent plastic deformation is presented in Fig 4.20, at the end of the calculation t = 1.1 s.

This distribution looks quite similar to that in Fig 4.17. In Case 1d the reinforcement yields somewhat more at the junction with the floor at level 25.00 compared with Case 1c.

Cracks at the outer and inner surface of the wall at the end of the calculation are shown in Figs 4.21 a and b. These crack distributions are almost equal to the corresponding distributions in Case 1c, Figs 4.18 a and b. There is cracking through the wall in the supporting floor area.

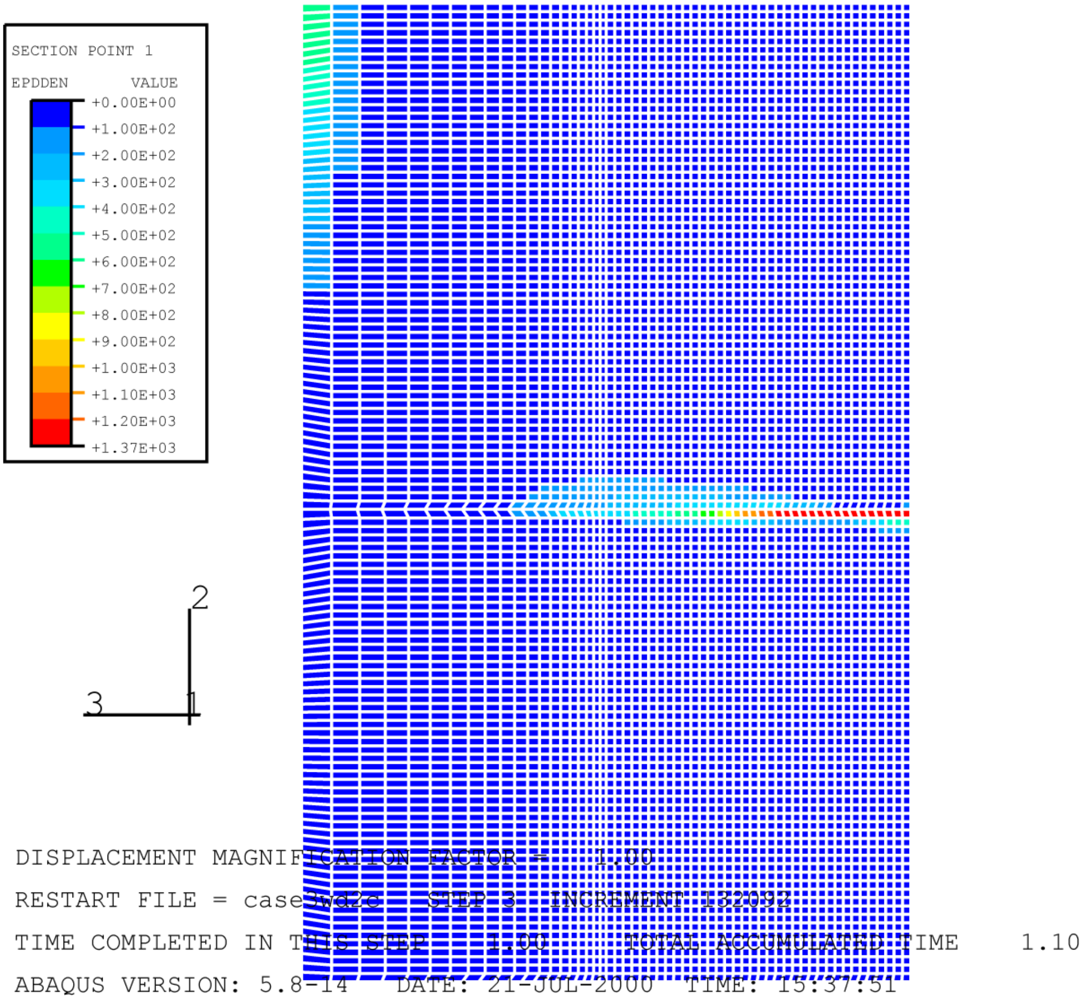

Figure 4.20. Total energy dissipated per unit volume by plastic deformation, Case 1d.

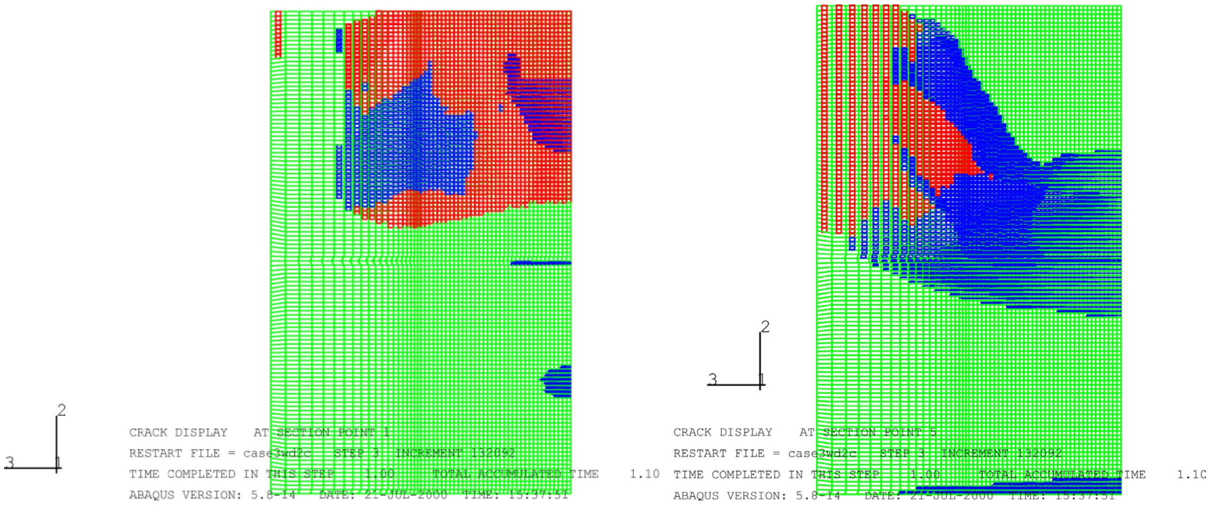

Figure 4.21. Cracks at the outer (a) and inner (b) surfaces at end of calculation, Case 1d.

4.3.2 Case 2

The effect of the detonation transient due to a 1.428 kg hydrogen detonation was studied when the detonation occurred in the upper location. The shock pressure transients corresponding to a detonation of 1.428 kg hydrogen at the upper location of the room are shown in Fig. 3.4b. Only the pressure increase before detonation and the detonation peak were simulated. Crack development at outer and inner surfaces of the wall is shown in Figs. 4.22 a-h.

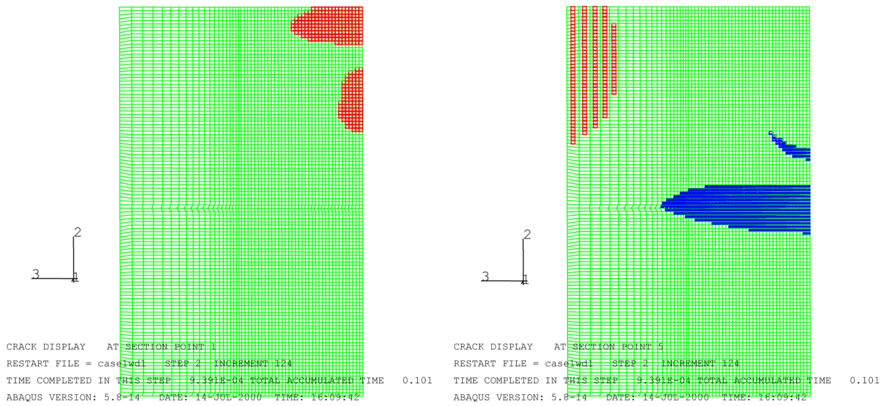

Figure 4.22 a, b. Cracks at the outer (a) and inner (b) surfaces, t = 0.101 s, Case 2.

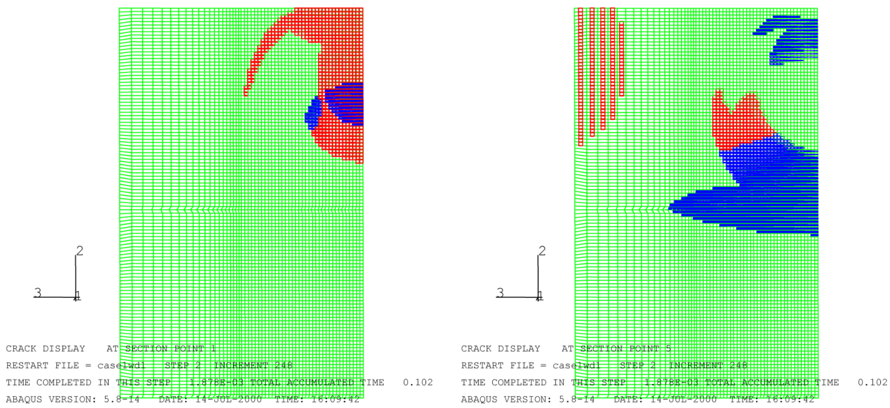

Figure 4.22 c, d. Cracks at the outer (c) and inner (d) surfaces, t = 0.102 s, Case 2.

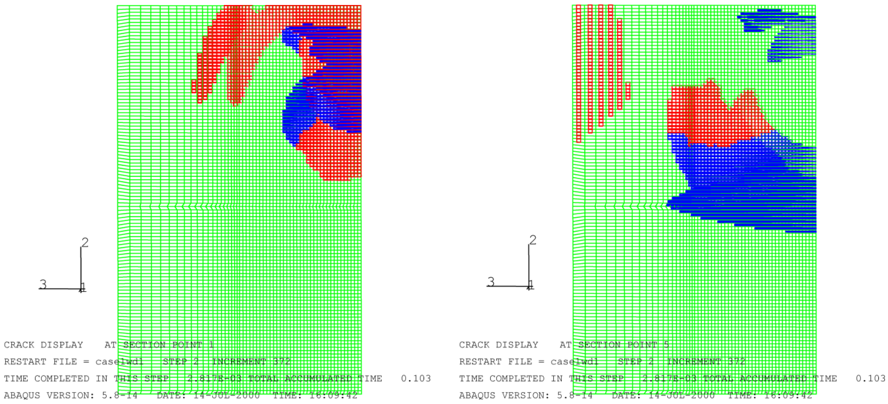

Figure 4.22 e, f. Cracks at the outer (e) and inner (f) surfaces, t = 0.103 s, Case 2.

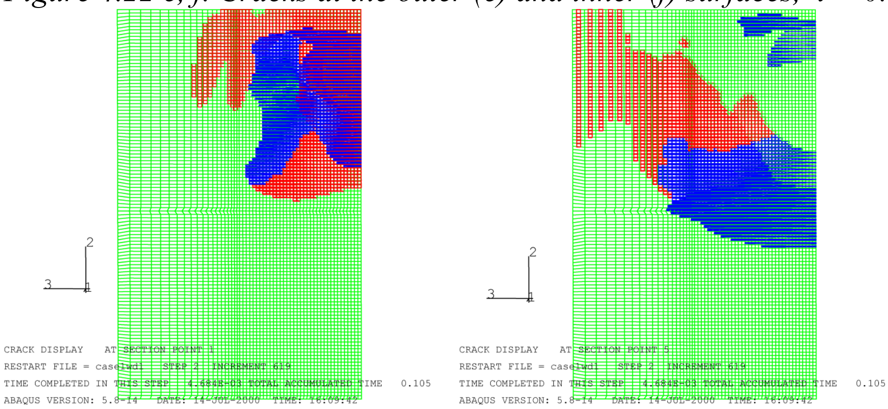

Figure 4.22 g, h. Cracks at the outer (g) and inner (h) surfaces, t = 0.105 s, Case 2.

The reinforcement starts to yield at the inner surface near the supporting floor at level 25.00. The compression strength of the concrete is exceeded at the outer surface of the wall.

4.3.3 Case 3

The effect of the detonation transient due to a 1.428 kg hydrogen detonation was studied when the detonation site was at the lower location. The shock pressure transients corresponding to a detonation of 1.428 kg hydrogen at the lower location of the room are shown in Fig. 3.4b. Cracking at the outer and inner surfaces of the wall is shown in Figs. 4.23 a-h.

The reinforcement starts to yield near the bottom of the model, at level 19.00. Also, stresses on the compressed surface do exceed the compression strength of the concrete.

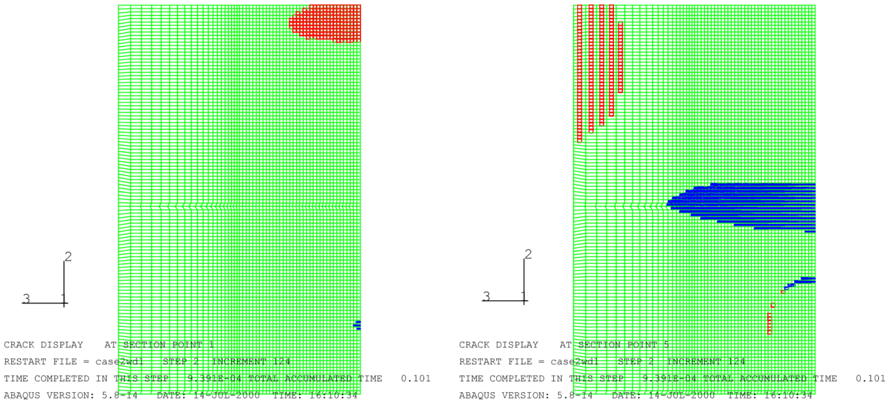

Fig. 4.23 a, b. Cracks at the outer (a) and inner (b) surfaces, t = 0.101 s, Case 3.

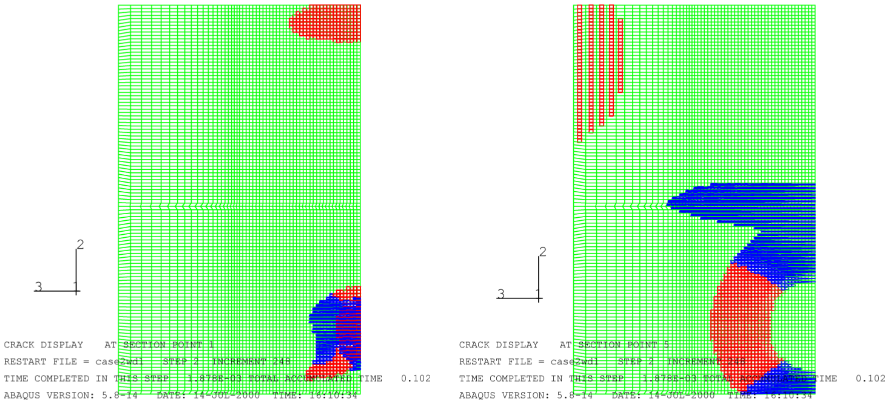

Fig. 4.23 c, d. Cracks at the outer (c) and inner (d) surfaces, t=0.102 s, Case 3.

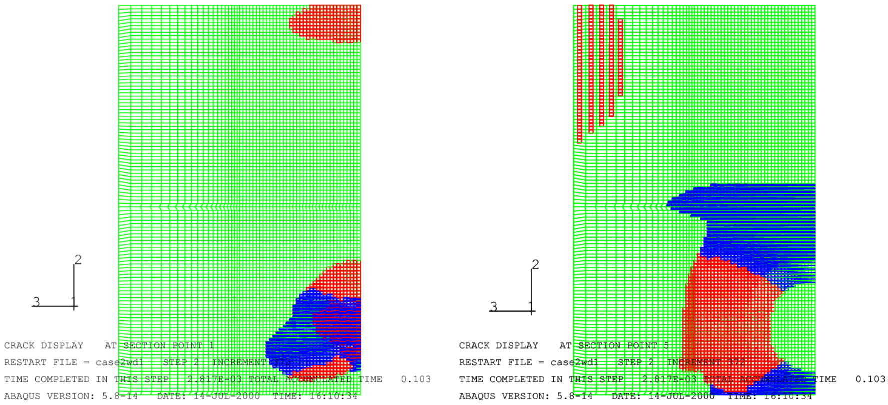

Fig. 4.23 e, f. Cracks at the outer (e) and inner (f) surfaces, t = 0.103 s, Case 3.

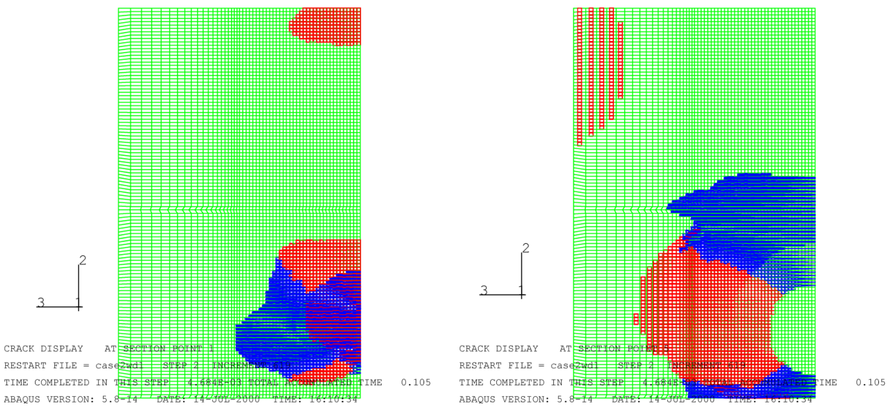

Fig. 4.23 g, h. Cracks at the outer (g) and inner (h) surfaces, t = 0.105 s, Case 3.

5 Criteria

The following phenomena should be considered when studying the load carrying capacity of a reinforced concrete structure:

Concrete cracking:	Cracks on surfaces
	Through cracked section
Concrete compression crushing	
Reinforcement:	Yielding
	Ultimate tensile strain (15%) exceeded.

Due to the low tensile strength of concrete, cracking on the surface starts at a relatively low loading level. Gradually, the tensile reinforcement carries more and more tensile stresses. Normally, in order to avoid catastrophic failure, the tensile reinforcement is designed to yield before the concrete crushes on the compressed surface.

In case the reinforcement does not yield, the elastic tensile strains will recover after a load decrease and tensile cracks will close. If there are plastic tensile deformations in the reinforcements, the cracks will not close completely even if there is no longer any loading.

6 Summary and Conclusions

The load carrying capacity of a reinforced concrete wall was studied. First, linear analyses were carried out and the moment capacities were evaluated based on codes and standards.

Materially non-linear analyses were carried out using simple boundary conditions for simulating the effect of surrounding structures.

Static non-linear analyses were carried out in order to assess the ultimate capacity of the wall under unified pressure. The ABAQUS/Standard program using the Riks method for the proportional loading procedure was applied for these analyses.

Dynamic materially non-linear analyses were carried out by ABAQUS/Explicit program. According to the preliminary analyses the wall may not resist a static-type pressure following the detonations considered. Some analyses were performed to find a relatively slow linearly decreasing pressure load which the wall could resist.

The non-linear behaviour of the wall was studied under detonations corresponding to a detonable hydrogen mass of 0.5 kg and 1.428 kg.

The wall seems to resist quite well the pressure increase before detonation. This pressure value is near the 'design load'. The duration of the detonation is brief compared with the eigenperiods of the wall. The wall may somehow survive the detonation peak transient, but the relatively slowly decreasing static type pressure after the peak detonation damages the wall much more severely than the detonation peak itself.

In calculating dynamic behaviour during a decreasing pressure after detonation, the amount of structural damping applied is important. During a rapid detonation simulation the effect of damping is negligible. Also, the parameter used in decreasing the tensile stresses to zero in cracked concrete calculation points affects the stress state of the reinforcement. In a case where the stresses are assumed to decrease to zero at a relatively small crack strain value, the tensile stresses will be transferred quite rapidly to the reinforcement. This is a conservative assumption but easily causes numerical problems in calculations. In order maintain the energy balance during analyses, in some parameter studies the zero stress crack strain value was assumed to be unrealistically high.

After extensive cracking the energy balance is easily lost, especially when the reinforcement starts to yield. Once the energy balance is lost in numerical analysis, the results are no longer reliable. Concrete compression crushing cannot be simulated by the ABAQUS/Explicit program.

References

ABAQUS Theory Manual. Version 5.8. 1998. Hibbit, Karlsson & Sorensen Inc. Rhode Island (RI).

ABAQUS/Explicit Lectures 1996. Analysis of Concrete Structures Using ABAQUS/Explicit. 1996.

Bathe, K.-J. & Wilson, E. L. 1976. Numerical Methods in Finite Element Analysis. Prentice Hall, Inc. 1976.

Betoninormit 1981. Finnish Concrete Standard. RIL 131-1981.

Boswell, L. F. & D'Mello, C. 1993. The Dynamics of Structural Systems. Blackwell Scientific Publications, Oxford.

Lindholm, I. 2000. Private Conversation.

Shayanfar, M. A., Kheyroddin, A. & Mirza, M. S. 1997. Element size effects in nonlinear analysis of reinforced concrete members. Computers & Structures, Vol. 62, No 2, pp. 339-352.

Silde, A. 1999. Program Interface for the DETO and ABAQUS Codes. Research Report ENE4/43/99.

Silde, A. & Lindholm, I. 2000. On Detonation Dynamics in Hydrogen-Air-Steam Mixtures: Theory and Application to Olkiluoto Reactor Building. Roskilde: NKS. 83 p. Report NKS-9. ISBN 87-7893-058-8.

Bibliographic Data Sheet **NKS-26**

Title	Reinforced concrete wall under hydrogen detonation
Author(s)	Arja Saarenheimo
Affiliation(s)	VTT Manufacturing technology, Finland
ISBN	87-7893-077-4
Date	November 2000
Project	NKS/SOS-2.3
No. of pages	45
No. of tables	7
No. of illustrations	46
No. of references	9

Abstract

The structural integrity of a reinforced concrete wall in the BWR reactor building under hydrogen detonation conditions has been analysed. Of particular interest is whether the containment integrity can be jeopardised by an external hydrogen detonation. The load carrying capacity of a reinforced concrete wall was studied. The detonation pressure loads were estimated with computerised hand calculations assuming a direct initiation of detonation and applying the strong explosion theory. The results can be considered as rough and conservative estimates for the first shock pressure impact induced by a reflecting detonation wave.
Structural integrity may be endangered due to slow pressurisation or dynamic impulse loads associated with local detonations. The static pressure following the passage of a shock front may be relatively high, thus this static or slowly decreasing pressure after a detonation may damage the structure severely. The mitigating effects of the opening of a door on pressure history and structural response were also studied. The non-linear behaviour of the wall was studied under detonations corresponding a detonable hydrogen mass of 0.5 kg and 1.428 kg.
Non-linear finite element analyses of the reinforced concrete structure were carried out by the ABAQUS/Explicit program. The reinforcement and its non-linear material behaviour and the tensile cracking of concrete were modelled. Reinforcement was defined as layers of uniformly spaced reinforcing bars in shell elements. In these studies the surrounding structures of the non-linearly modelled reinforced concrete wall were modelled using idealised boundary conditions. Especially concrete cracking and yielding of the reinforcement was monitored during the numerical simulation.

Key words: Non-linear reinforced concrete, hydrogen detonation, finite element analysis

Available on request from the NKS Secretariat, P.O.Box 30, DK-4000 Roskilde, Denmark.
Phone (+45) 4677 4045, fax (+45) 4677 4046, e-mail nks@catscience.dk, www.nks.org.